Cyclodextrin-assisted low-metal Ni-Pd/Al2O3 bimetallic catalysts for the direct amination of aliphatic alcohols

Ajay Tomer, Bright Kusema, Jean-François Paul, Cédric Przybylski, Eric Monflier, Marc Pera-Titus, Anne Ponchel

Cyclodextrin-assisted low-metal Ni-Pd/Al_2O_3 bimetallic catalysts for the direct amination of aliphatic alcohols

Ajay Tomer,[1,2] Bright T. Kusema,[2] Jean-François Paul,[1] Cédric Przybylski,[3] Eric Monflier,[1] Marc Pera-Titus [2]* and Anne Ponchel [1]*

[1] Univ. Artois, CNRS, Centrale Lille, ENSCL, Univ. Lille, UMR 8181, Unité de Catalyse et de Chimie du Solide (UCCS), F-62300 Lens, France.

[2] Eco-Efficient Products and Processes Laboratory (E2P2L), UMI 3464 CNRS – Solvay, 3966 Jin Du Road, Xin Zhuang Ind. Zone, 201108 Shanghai, China.

[3] Sorbonne Universités, CNRS, Institut Parisien de Chimie Moléculaire, UMR 8232, 4 Place Jussieu, 75005, Paris, France.

*Corresponding author: *anne.ponchel@univ-artois.fr*

*Corresponding author: *marc.pera-titus-ext@solvay.com*

Abstract

This paper reports the use of β-cyclodextrin as a pre-shaping agent for the preparation of low-metal xNi-yPd/Al_2O_3 catalysts (x = 2, 5 wt.% and y = 0.2, 0.5, 1.0 wt.%) for the direct amination of 1-octanol with ammonia. Six different preparation methods were used aiming at tuning the Ni-Pd interaction. The catalysts were finely characterized by XRD, H_2-TPR, CO pulse chemisorption, STEM-EELS/EDS-SDD and XPS, while the elementary interaction between Ni-Pd-cyclodextrin was assessed by marrying ESI-MS experiments with DFT calculations. Among the different methods studied, the most outstanding effect was obtained when β-cyclodextrin was pre-adsorbed on γ-Al_2O_3 before impregnating the Ni and Pd nitrate precursors. At such conditions, the best formulation (5Ni-0.5Pd/Al-CD_M4) afforded 90% conversion and 71% yield to 1-octylamine (TON = 93) in the amination of 1-octanol with ammonia at 160 ºC for 4 h, which places it among the most active and selective Ni catalysts reported in the literature.

Keywords

• Octanol • Ammonia • Direct amination • Borrowing hydrogen • Cyclodextrin • Ni-Pd alumina

1. Introduction

Alkylamines derived from fatty acids, olefins or alcohols are relevant chemical intermediates for the manufacture of agrochemicals, surfactants and polymers [1,2]. The world market of alkylamines is segmented in 6 sectors: (1) water treatment, (2) agrochemistry, (3) oilfield, (4) asphalt additives, (5) anti-caking, and (6) others (personal care, mining, fabric softening, paints and coatings) [3]. Among the different technologies for producing amines, the alkylation of amines with (bio)alcohols appears as an eco-efficient method for amine production as water is generated as the main byproduct [4].

The most extended catalysts for the direct synthesis of amines from alcohols rely on homogeneous Ru and Ir complexes operating *via* the borrowing H_2 or H_2 auto-transfer mechanism without external H_2 supply [5-8]. In parallel, heterogeneous catalysts based on Raney Ni [9,10] and Ni nanoparticles (*e.g.*, Ni [11-17] and NiCu [18-21], $NiCuFeO_x$) supported over alkaline or amphoteric oxides have shown high versatility for the alkylation of amines and ammonia with aromatic and aliphatic alcohols. The major shortcoming of Ni formulations is often ascribed to the large Ni content (most often >15 wt.%), as well to the heterogeneous particle size distributions and low metal dispersion, which impact the activity for amination. Furthermore, highly Ni loaded catalysts are prone to leaching upon exposure to ammonia and polar solvents, thereby affecting not only the catalytic activity, but also potentially polluting the amine product by Ni contamination. Also noteworthy, catalysts with Ni contents as low as 2 wt.% are hardly active due to the absence of surface Ni species and formation of inactive nickel aluminate species [22,23]. Accordingly, the development of eco-efficient processes with stable and selective heterogeneous catalysts with low Ni contents for the direct amination of alcohols is highly desired.

Even if Pd and Ni belong to the same group in the periodic table (group 10, d^{10} or d^8s^2) both transition metals behave differently over alumina. Pd is usually dispersed in the form of PdO_x and tends to form aggregates at high temperature (>800 ºC) [24], whereas Ni can be dispersed forming

a variety of oxide species (i.e. bulk NiO, surface NiO and nickel aluminates) with variable interaction with alumina as a function of the thermal treatment (calcination and reduction under H_2) [25]. Interestingly, bimetallic NiPd catalysts have been reported to show superior activity than the corresponding monometallic counterparts in hydrogenation reactions, which can be ascribed to either electronic effects, or to a promoted reducibility of Ni [26-29]. Despite these potential benefits, NiPd bimetallic systems have been seldom explored for the amination of aliphatic alcohols. The first example was reported in the patent by Vedage et *al*. (Air Products) disclosing a bimetallic PdNi catalyst comprising 15-20 wt.%Ni and 0.5-3 wt.% Pd over alumina, silica and titania for the amination of 1-butanol with ammonia [12]. PdNi catalysts not only exhibited higher activity, but also could be reduced at a significantly lower temperature (200 ^{o}C *vs.* 400 ^{o}C) compared to monometallic Ni catalysts with a similar Ni content (15 wt.%). It clearly emerges from these different reports that the promotion of Ni-supported catalysts by Pd might be of interest for engineering new catalysts based on low-Ni content for the direct amination of alcohols.

In recent work, we have shown that the addition of small quantities of cyclodextrins (in particular β-CD composed of seven α-D glucopyranose units) during the preparation of Ni-supported catalysts by wet impregnation could drastically enhance the catalytic performance in the direct amination of alcohols by promoting the formation of more reducible and smaller nickel oxide particles enriched with surface Ni species [30]. This effect was particularly pronounced for a β-CD/Ni molar ratio close to 0.1 and could be preserved over a wide range of Ni loading (5-20 wt. %). The beneficial effect of β-CD was mainly related to its ability to spontaneously form complexes with the Ni precursor in the impregnation aqueous solution. This interaction is driven by the numerous hydroxyl groups present on the CD torus which, during the calcination, decrease the interaction of Ni^{2+} and Al^{3+} ions responsible for the formation of hard-to-reduce nickel aluminates species and limit the growth of nickel oxide particles over the alumina support.

On the guidance of the above recent findings, herein we report the use of β-CD for the preparation of $NiPd/Al_2O_3$ bimetallic catalysts encompassing low Ni content (2 or 5 wt.%). To this aim,

a series of catalysts have been synthesized by aqueous wet impregnation of nickel and palladium nitrate salts using β-CD as supramolecular additive. The impact of β-CD has been explored using various synthetic protocols differing one another from the order of addition of the reagents. The ability of β-CD to condition the final structure of bimetallic catalysts is discussed in detail on the basis of ESI-MS data combined with DFT calculations in solution, together with XRD, H_2-TPR, XPS, CO pulsed chemisorption and STEM-EELS/EDS of the calcined catalysts. The catalytic performance has been assessed in the liquid-phase amination reaction of 1-octanol with ammonia, aiming at producing the targeted primary amine, *i.e.* 1-octylamine.

2. Experimental

2.1. Materials

γ-Al_2O_3 (Puralox SASOL Scca-5/170, 154 m^2/g) was procured from SASOL North America Inc. (Houston, USA) and was used as received without any further treatment for preparing the Ni-Pd supported catalysts. Palladium nitrate dihydrate ($Pd(NO_3)_2.2H_2O$, 40 wt.% Pd) and nickel nitrate hexahydrate ($Ni(NO_3)_2.6H_2O$, purity >99.9 wt.%), both purchased from Sigma-Aldrich, were used as precursors for the synthesis of bimetallic catalysts. Native cyclodextrin (β-CD) was supplied by Roquette Frères (Lestrem, France). All other reactants and solvents were obtained from J&K Chemicals in their highest purity (purity 99.5%) and were used without any further purification or drying.

2.2. Catalyst synthesis

A series of Ni-Pd bimetallic catalysts supported over γ-Al_2O_3, denoted as xNi-yPd/Al_M and xNi-yPd/Al-CD_M with x = 2 and 5 wt.%, y = 0.2, 0.5 and 1.0 wt.% were prepared by different methods ranging from M1 to M6, all being based on wet impregnation. The principle of the preparation methods of Ni-Pd catalysts is shown schematically in Figure 1. These methods differ from the use (or not) of β-CD and from the impregnation mode, either by direct co-impregnation over

the alumina support using co-mixed Ni and Pd salts, or by sequential impregnation of the Pd salt to NiO/Al_2O_3 with or without β-CD. The detailed protocols for catalysts synthesis are provided in the following lines.

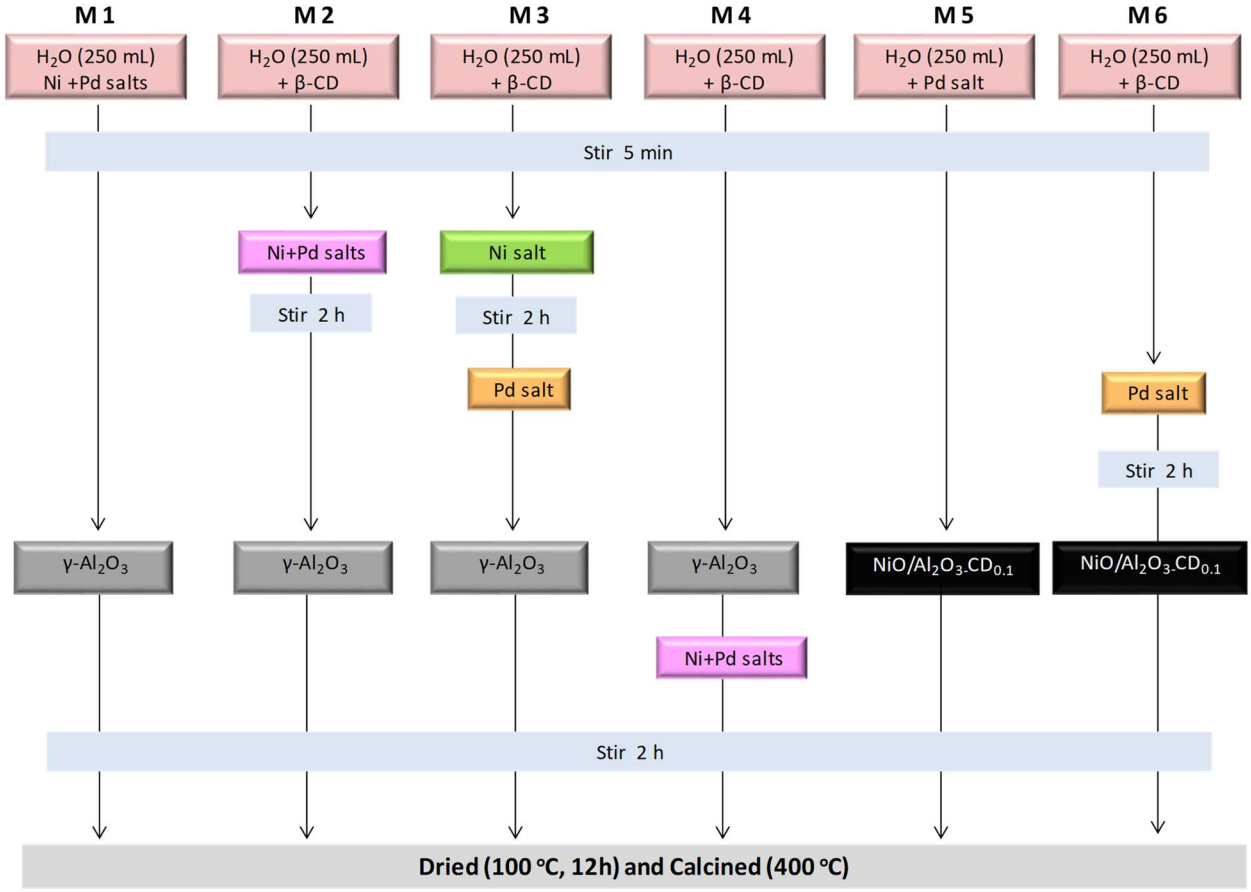

Figure 1. Methods for the preparation of Ni-Pd/Al catalysts by wet impregnation without (M1) and with using β-CD (M2, M3, M4, M5 and M6).

2.2.1. Method 1 (M1)

The *x*Ni-yPd/Al_M1 catalysts were synthesized by direct co-impregnation without β-CD. In this protocol, a given amount of nickel and palladium nitrate salts was dissolved in 250 mL of distilled water and stirred for 5 min. Subsequently, γ-Al_2O_3 (5 g) was added and the suspension was stirred at room temperature for 2 h. The water excess was slowly removed using a rotary evaporator at 60 °C until dryness. The recovered solid was then dried overnight in an oven at 100 °C and calcined at 400 °C for 4 h using a heating rate of 2 °C min^{-1} under 2 L(STP) h^{-1} airflow.

The catalysts synthesized by this method were denoted as 2Ni-0.2Pd/Al_ M1, 5Ni-0.5Pd/Al_M1 and 5Ni-1.0Pd/Al_M1.

2.2.2. Method 2 (M2)

The *x*Ni-*y*Pd/Al-CD_M2 catalysts were synthesized in the presence of β-CD as follows. An aqueous mixture of nickel nitrate hexahydrate (1.310 g) and palladium nitrate dihydrate (0.0661 g for y = 0.5 wt.% or 0.132 g for y = 1.0 wt.%) was added simultaneously to 250 mL of an aqueous solution containing 0.511 g of native β-CD (0.1 mol equiv with respect to Ni). This solution was kept under constant stirring at room temperature for 2 h. Subsequently, γ-Al_2O_3 (5 g) was added and the solid suspension was stirred for another 2 h. The excess water was then slowly removed using a rotary evaporator at 60 ^oC until dryness. The post-treatment procedure (drying and calcination) was similar to that described in Method 1. The catalysts prepared by this method were denoted as 5Ni-0.5Pd/Al-CD_M2 and 5Ni-1.0Pd/Al-CD_M2.

2.2.3. Method 3 (M3)

Method 3 consists of a modified version of Method 2. In this method, 0.5109 g of β-CD (0.1 mol equiv with respect to Ni) were first added to 250 mL of distilled water and stirred for 5 min. Then, 1.310 g of nickel nitrate hexahydrate salt was added and the solution was stirred for 2 h. After this period, 0.0661 g of palladium nitrate dihydrate salt was quickly introduced and the solution was stirred for 2 min immediately followed by the addition of γ-Al_2O_3 (5 g). The solid suspension was stirred at room temperature for another 2 h. Then, the excess water was slowly removed using a rotary evaporator at 60 ^oC until dryness. The post-treatment procedure (drying and calcination) was analogous to that described in Method 1. The catalyst synthesized by this method was denoted as 5Ni-0.5Pd/Al-CD_M3.

2.2.4. Method 4 (M4)

In this method, 0.5109 g of β-CD (0.1 mol equiv with respect to Ni) were first added to 250 mL of distilled water and stirred for 5 min followed by the addition of γ-Al_2O_3 (5 g). The γ-

Al_2O_3/β-CD suspension was stirred for another 5 min. The bimetallic solution (1.310 g Ni nitrate salt and 0.0661 g Pd nitrate salt) was then introduced and the resulting suspension was stirred at room temperature for 2 h. After this period, the excess water was slowly removed using a rotary evaporator at 60 ºC until dryness. The post-treatment procedure (drying and calcination) was similar to that described in Method 1. The catalysts synthesized by this method were denoted as 5Ni-0.5Pd/Al-CD_M4. For the sake of comparison, a low-metal loaded catalyst (2 wt.% Ni and 0.2 wt.% Pd) was also prepared using this procedure by adjusting the quantities of reagents to 5 g of Al_2O_3. This catalyst was denoted as 2Ni-0.2Pd/Al-CD_M4.

2.2.5. Method 5 (M5)

This method relies on the sequential impregnation of the Pd precursor over Ni/Al_2O_3. First, a monometallic 5Ni/Al-β-$CD_{0.1}$ catalyst was prepared by wet impregnation as described elsewhere [30]. In short, the nickel nitrate salt (1.310 g) was added to 250 mL of an aqueous solution containing 0.1 equiv of β-CD followed by 2 h stirring at room temperature. After this period, 5 g of γ-Al_2O_3 was added to the above solution and stirred for 2 h. Water was then removed and the solid was dried in an oven and calcined at 400 ºC for 4 h. Subsequently, 5 g of the calcined catalyst (5Ni/Al-β-$CD_{0.1}$) were introduced to a solution of 0.0661 g palladium nitrate dihydrate salt in 250 mL of distilled water and the solid suspension was stirred for 2 h. The remaining post-treatment procedure was identical to that described in Method 1 (water removal, drying and calcination at 400 ºC under air). The catalyst synthesized by this method was denoted as 5Ni-0.5Pd/Al-CD_M5.

2.2.6. Method 6 (M6)

Method 6 was very similar to Method 5 differing only from the second step of the protocol, where Pd impregnation (0.0661 g) was carried out in the presence of β-CD (0.1 mol equiv with respect to Pd). Overall, β-CD was used twice, *i.e.* during Ni/Al_2O_3 synthesis and during Pd impregnation over the calcined 5Ni/Al-β-$CD_{0.1}$. The catalyst synthesized by this method was denoted as 5Ni-0.5Pd/Al-CD_M6.

2.2.7. Monometallic catalysts (control catalysts)

In addition to bimetallic catalysts, a series of control monometallic catalysts was prepared, *i.e.* 2Ni/Al, 2Ni/Al-β-$CD_{0.1}$, 5Ni/Al, 5Ni/Al-β-$CD_{0.1}$, 0.5Pd/Al, 0.5Pd/Al-β-$CD_{0.1}$, by wet impregnation using nitrate precursor salts with or without the presence of β-CD. In all cases, the solids recovered after the impregnation step and water removal were dried in an oven at 100 ºC and calcined under an air flow [2 L(STP)/h] at 400 ºC for 4 h using a heating rate of 2 ºC.min^{-1}.

2.3. Catalyst characterization

The bulk metal composition of the calcined catalysts was measured by Inductively Coupled Plasma-Optical Emission Spectrometry using a 720-ES ICP-OES Agilent instrument. Before the analyses, the dried and grounded sample (10 mg) was dissolved in 2.4 mL of concentrated *aqua regia* and this solution was heated to 110 ºC for 3 h. Then another 2 mL of concentrated *aqua regia* was added to the solution, which was kept at 60 °C for 1 h to ensure complete digestion. Finally, the volume was adjusted to 20 mL using ultrapure water in the presence of 100 µL of an internal standard before ICP-OES analysis. All analyses were performed in triplicate and the results were represented as mean ± standard deviation.

The specific surface area and pore volume of the catalysts were measured from the N_2 adsorption/desorption isotherms at -196 ºC using a Micromeritics ASAP 2010 Surface Area Analyzer. The surface areas were calculated by the Brunauer-Emmett-Teller (BET) method in the relative pressure range $0.05 < P/P_0 < 0.25$, while the pore volumes were measured at $P/P_0 = 0.99$. The Barrer-Joyner-Halenda (BJH) method was used for measuring the interparticle pore size distributions. Before the measurements, the catalysts were degassed overnight at 100 ºC.

The electrospray-mass spectrometry (ESI-MS) experiments were conducted on a LTQ-Orbitrap XL instrument from Thermo Scientific (San Jose, CA, USA) operated in positive ionization mode with a spray voltage at +3.85 kV and an auxiliary gas flow at 45 and 15 a.u., respectively. The applied voltages were +40 V and +100 V for the ion transfer capillary and the tube lens,

respectively. The ion transfer capillary was held at 275 °C and a resolution of 30,000 (*m/z* = 400) was applied. Stock solutions of β-CD and nickel/palladium nitrate were prepared in methanol/water (1:1 v/v) at 1 mM and 200 mM respectively. Then, each solution was diluted in methanol/water (1:1 v/v) to give the final analytical solutions of β-CD at 10 µM with nickel nitrate and/or palladium nitrate at the desired concentrations. Once prepared, the fresh solutions were continuously infused at 5 µL.min^{-1} using a 250 µL syringe. The high-energy collision dissociation (HCD) experiments were conducted with an activation time of 100 ms according to a previous study [31,32] and the normalized collision energy (NCE) varied from 0 to 50% with a precursor selection window set to *m/z* =2.5 during the MS experiment.

The phases present in the catalysts were analyzed by powder X-ray diffraction (PXRD). The PXRD patterns were recorded on a Bruker D8 Advance diffractometer in Bragg-Brentano geometry equipped with a copper anode (λ = 1.5418 Å) and a 1D PSD Lynxeye detector. The patterns were collected in the 2θ range 8-80° with a step size of 0.02°. The patterns were indexed using the Joint Committee on Powder Diffraction (JCPDS) database and interpreted using MDI JADE 5.0 software. The Scherrer equation was used to estimate the average size of the oxide particles from the XRD line broadening.

H_2-temperature-programmed reduction (H_2-TPR) was used to assess the reducibility of the catalysts. The reduction profiles were measured on a Micromeritics AutoChem 2920 instrument equipped with a thermal conductivity detector (TCD) and a cold trap before the detector. The H_2-TPR profiles were recorded by reducing the samples (75 mg) under 10%H_2-Ar flow [40 mL(STP)/min] in the temperature range 30-1000 ºC and from -60 ºC to 1000 ºC starting at cryogenic conditions using in all cases a heating rate of 10 ºC.min^{-1}. The H_2 consumption was used to measure the reduction level of the different nickel and palladium oxide species present in the calcined samples.

Pulse CO chemisorption measurements were carried out using a Micromeritics AutoChem 2920 instrument. Briefly, a known quantity of the calcined catalyst (100 mg) was reduced under a

10% H_2-Ar flow [40 mL(STP)/min] at 580 ºC for 30 min using a heating rate of 10 ºC.min^{-1}. Then, the sample was cooled down to 50 ºC followed by purging under He [20 mL(STP)/min] for 20 min and then CO chemisorption analysis was performed by introducing successive 10% CO-He pulse doses until no further CO uptake was measured. The CO uptake afforded the measurement of the metal dispersion (%D), the metal surface area per gram of catalyst and per gram of metal (A_m), and the average particle size of the metal (S_m). The stoichiometry factor S. F. between the metal atoms and CO molecules was assumed to be 2 [33].

The morphology and local composition of the catalysts were characterized by STEM-EELS/EDS using a 200 kV Tecnai F20 microscope equipped with a FEG electron gun, a STEM unit and an EDAX Optima T60 SDD-EDS spectrometer. The micrographs were analyzed using EDAX Team microanalysis software. Before the analyses, the solid powder was directly dispersed over the holey carbon Cu 400 mesh grid (Agar, Ref S147-4).

The surface composition of the catalysts was analyzed by X-ray photoelectron spectroscopy (XPS) using a Kratos Axis Ultra DLD apparatus equipped with a hemispherical analyzer and a delay line detector. The spectra were recorded using an Al monochromated X-ray source (10 kV, 15 mA) with a pass energy of 40 eV (0.1 eV/step) for high resolution spectra, and a pass energy of 160 eV (1 eV/step) for survey spectrum in hybrid mode and slot lens mode, respectively. The adventitious C1s binding energy (285.0 eV) was used as an internal reference. Prior to the measurements in the calcined state, the samples were treated at 300 °C for 30 min under airflow [50 mL(STP).min^{-1}] in the pre-treatment chamber, whereas for the measurements in the reduced state, the samples were treated in the same pre-treatment chamber at 580 °C for 30 min under a diluted H_2 flow [5 vol.% H_2 in Ar, 50 mL(STP).min^{-1}].

2.4. DFT calculations

Spin unrestricted DFT calculations were performed using VASP 5.5.1 software [34-37]. PBE functionals were used to compute the energy of the systems, whereas PAW pseudo potentials were

employed to describe core electrons and the region close to the nucleus of valence electrons [38,39]. The number of valence electrons was 1, 4, 6, 10 and 10 for H, C, O, Ni and Pd elements, respectively. The cutoff energy was set to 450 eV. The geometry of β-CD and the different metal complexes was fully optimized without any constraints using a 25 x 25 x 25 $Å^3$ cubic cell. Due to the size of the cell, the integration in the reciprocal space was done at the Gamma Kpoint. The PCM model developed by Hennig was used to assess the influence of the solvent [40,41].

2.5. Catalytic activity measurements

The catalytic activity of the bimetallic catalysts was assessed in the amination of 1-octanol with NH_3 (Scheme 1).

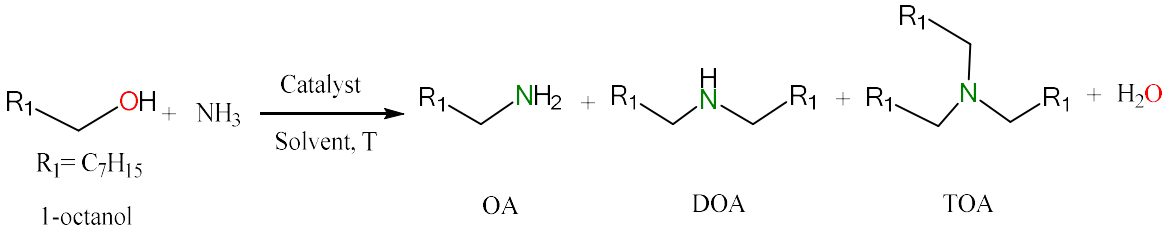

Scheme 1. Potential amination products in the reaction between 1-octanol with NH_3.

In a typical experiment, the reactor, a 30-mL stainless steel autoclave equipped with a magnetic stir bar and a heating mantle, was charged with 1-octanol (1.3 mmol) and 60 mg of pre-reduced catalyst. The reactor was sealed and evacuated by applying vacuum followed by charging NH_3 (7 bar). The reactor was then placed on a magnetic stirring hot plate at 160 ºC for 4 h. At these conditions, the nominal NH_3/1-octanol molar ratio in our reactor was 25, whereas the NH_3/1-octanol molar ratio in the reaction zone was about 19 given the configuration and temperature distribution in the reactor. The reactant (1-octanol) and the expected products, *i.e.* 1-octylamine (OA), dioctylamine (DOA), trioctylamine (TOA), octanenitrile (ON) were quantified by gas chromatography using an Agilent 7890 GC equipped with a HP-5 capillary column with 5 wt.% phenyl groups and biphenyl as internal standard. The conversion of the limiting reactant (LR: 1-octanol)

and the selectivity, yield to the N-containing products and carbon balance were defined as follows :

$$\text{Conversion}(\%) = 1 - \frac{n_{LR}}{n_{LR}^{0}} \quad (1)$$

$$\text{Selectivity}_i(\%) = \frac{n_i}{n_{LR}^{0} - n_{LR}} \quad (2)$$

$$\text{Yield}_i(\%) = \frac{n_i}{n_{LR}^{0}} \quad (3)$$

$$\text{Carbon balance} = \frac{\text{Moles of formed products + reactants}}{\text{Moles of reactants}} \quad (4)$$

where n_{LR}^{0} and n_{LR} refer to the initial and final mole number of the limiting reactant, respectively, whereas n_i corresponds to the mole number of N-containing products formed. Finally, the turnover number (TON) at a given time was computed by dividing the number of moles of OA formed by the total number of moles of surface Ni and Pd determined by CO-pulse chemisorption as follows

$$\text{TON} = \left(\frac{\text{Moles of formed OA}}{\text{Moles of Ni}_{surf} + \text{Pd}_{surf}} \right) \quad (5)$$

3. Results and discussion

3.1. Characterization

3.1.1. Study of metal-CD complex formation

The interaction between Ni and Pd, either individually or combined, with β-CD in solution was studied using electrospray mass spectrometry (ESI-MS) in positive mode. The solutions were prepared by mixing nickel and/or palladium nitrate precursors in the presence of β-CD (0.1 mol equiv with respect to metal) in aqueous methanol (1:1 v/v).

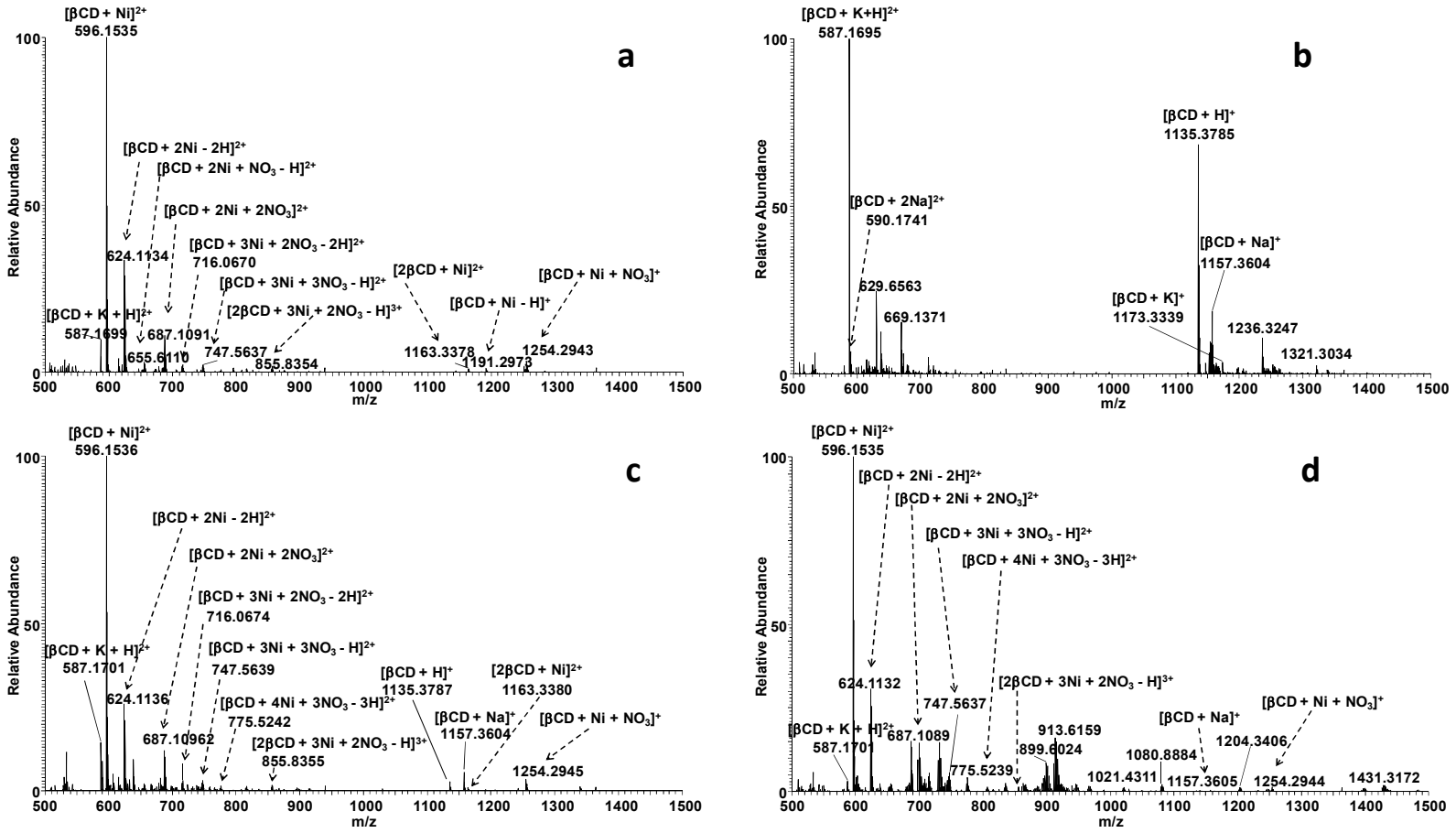

Figure 2. Positive electrospray mass spectra of β-CD mixed separately or together with Ni and Pd precursors at different molar concentrations in methanol/water (50% v/v): a) β-CD+$NiNO_3$ (10 μM :100 μM), b) β-CD + $PdNO_3$ (10 μM :100 μM), c) β-CD + $NiNO_3$ + $PdNO_3$ (10 μM :50 μM :50 μM) and d) β-CD + $NiNO_3$ + $PdNO_3$ (10 μM :100 μM :10 μM).

Figure 2 collects the ESI positive mass spectra obtained for Ni and Pd separately and for mixed Ni-Pd solutions at different concentrations. Figure 2a shows the mass spectrum of the solution containing nickel nitrate and β-CD. Among the different complex ions formed, the most intense ion appears at *m/z* 596.15, which can be assigned to $[\beta\text{-CD+Ni}]^{2+}$. The presence of this ion strongly supports the favorable interaction of β-CD with Ni in aqueous medium. Further evidence of complexation can be inferred from the presence of additional $[\beta\text{-CD+2Ni-2H}]^{2+}$ and $[2\beta\text{-CD+Ni}]^{2+}$ ions at *m/z* 624.11 and 1163.33, respectively. Additional positively charged complex ions of lower intensity can also be observed, such as at *m/z* 655.61, *m/z* 687.10, *m/z* 747.56 and *m/z* 855.83, being ascribed to $[\beta\text{-CD+2Ni+NO}_3\text{-H}]^{2+}$, $[\beta\text{-CD+2Ni+2NO}_3]^{2+}$, $[\beta\text{-CD+3Ni+3NO}_3\text{-H}]^{2+}$ and $[2\beta\text{-CD+3Ni+2NO}_3\text{-H}]^{3+}$, respectively.

A completely different complexation pattern is observed when nickel nitrate is replaced by palladium nitrate in the β-CD solution at the same molar ratio (0.1) (Figure 2b). The two most intense ions in the ESI-MS spectrum appear at *m/z* 1135.37 and 587.16, which are attributable to monoprotonated and doubly charged with both proton was and potassium β-CD [*i.e.*, $\beta\text{-CD +H}]^{2+}$ and $[\beta\text{-CD+K +H}]^{+}$), respectively [32]. Other minor ions are observed at *m/z* 590.17 and *m/z* 1157.36 corresponding to sodium adducts, such as $[\beta\text{-CD+2Na}]^{2+}$ and $[\beta\text{-CD+Na}]^{+}$. Surprisingly, no ionic complexes revealing the presence of any ion-molecule interactions between Pd(II) and β-CD is detected. The absence of formation of Pd(II)/β-CD adducts has been further confirmed by additional experiments using samples containing both Ni and Pd nitrate salts in a mixture with aqueous β-CD. Two mixtures were prepared in the presence of β-CD at a defined concentration (10 μM), one with molar concentrations of 50 μM Ni^{2+} and 50 μM Pd^{2+} (Figure 2c) and another with 100 μM Ni^{2+} and 10 μM Pd^{2+} (Figure 2d). As can be observed, the spectrum measured for both samples at low Pd concentration is very similar to that shown in Figure 2a accounting for the formation of ions corresponding to only complexes between β-CD and Ni. Moreover, no complex between β-CD and Pd is detected even after increasing the Pd concentration to the same level as

that of the Nickel salt (50 μM) (Figure 2c). Overall, these results clearly point out the more favorable interaction between β-CD and Ni than with Pd in our analytical conditions.

To gain more insight into the stabilizing effect of β-CD for Ni and Pd, a series of DFT calculation were conducted. Opposing the experimental results, the DFT calculations, which take into account both electrostatic interactions and orbital overlapping, predict that both metals should be equally stabilized by β-CD through the electron-donating oxygen atoms belonging to the hydroxyl groups located on the external rims. Figure S1 and Figure S2 collect all the tested complex geometries by DFT that can be formed between β-CD and Ni (starting from $[Ni(H_2O)_6]^{2+}$) or Pd (starting from $[Pd(H_2O)_4]^{2+}$) [42]. The most stable geometries are represented in Figure 3, while the corresponding interaction energies are collected in Table 1.

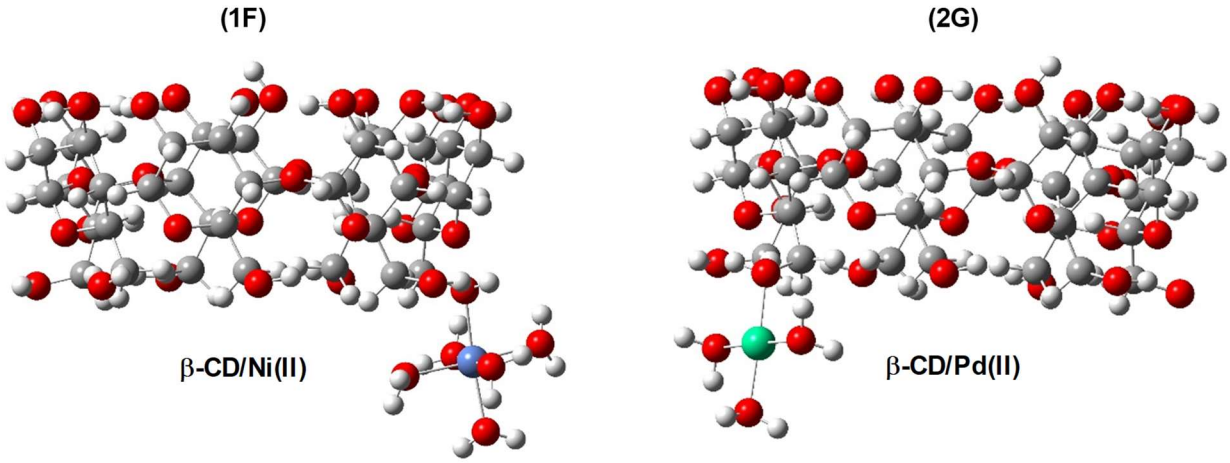

Figure 3. Model of the most stable complexes formed between β-CD and nickel (conformer 1F) and between β-CD and palladium (conformer 2G), both showing a stabilization by one electron-donating oxygen of the 6-hydroxyl group localized on the primary rim edge while keeping the cation outside the cavity. Color labels: nickel (blue), palladium (green), carbon (grey), oxygen (red) and hydrogen (white). The corresponding interaction energies are listed in Table 1.

Table 1. Interaction energies in eV calculated for the complex structures 1A-1F between nickel oxocation and native β-CD (Figure S1) and 2A-2G Pd^{2+} and β-CD (Figure S2)

	Interaction energy (eV)		Interaction energy (eV)
β-CD/Ni^{2+}		**β-CD/Pd^{2+}**	
1A	+0.27	2A	+0.21
1B	-0.59	2B	-0.34
1C	-0.36	2C	+0.33
1D	+1.13	2D	-0.56
1E	+0.058	2E	-0.29
1F	-0.75	2F	-0.48
		2G	-0.72

For both metals, the most stable complex is formed when one water molecule bonded to the metal center is substituted by a primary hydroxyl group (O6) located on the smaller rim of β-CD. The computed interaction energy is similar for both metals with a value of -0.75 eV for Ni and -0.72 eV for Pd (structures 1F and 2G in Figure 3, respectively), reflecting in both cases a comparable stability. This similarity can be related to the fact that Ni(II) and Pd(II) cations (transition metals of the same group in the periodic table, Ni being located just above Pd) are characterized by an identical external electronic structure, leading to only to slight changes in energy. We also considered other types of coordination, for instance through secondary hydroxyl atoms (O2 and O3). The formation of bidentate complexes (where the metal is coordinated to two secondary hydroxyl groups of β-CD *via* either the same glucopyranose unit or adjacent glucopyranose units) is less favorable, but still possible (-0.59 eV and -0.36 eV for Ni in structures 1B and 1C, and -0.56 eV and -0.29 eV for Pd in structures 2D and 2E). The only significant difference between Ni and Pd is observed when the metal is placed at the center of the β-CD cavity. As a matter of fact, the complexation process is endothermic in the case of Ni (+0.27 eV, structure 1A), while it is exothermic for Pd (-0.34 eV, structure 2B), forming in the latter case a host-guest complex through the penetration of the square planar Pd(II) complex along the axial line of the β-CD cavity. The inclusion phenomenon may be the result of combined effects between an enhanced electrostatic

interaction and a better size/shape-fit relationship on the basis of a less sterically crowded coordination environment for $[Pd(H_2O)_4]^{2+}$ compared to the octahedral $[Ni(H_2O)_6]^{2+}$ geometry [43,44].

The discrepancy between the ESI-MS data and the computational predictions cannot only be explained on the basis of thermodynamic considerations. Indeed, kinetic effects appear to come at play. The difference in the complexation ability between β-CD with Ni and/or Pd suggests that, under our experimental conditions, water exchange with the hydroxyl groups present on the β-CD rim would be mainly governed by the reaction kinetics on the metal sites. As a matter of fact, as previously reported [42], the exchange reaction rate is highly dependent on the nature of the metal ions, this being two orders of magnitude faster for $[Ni(H_2O)_6]^{2+}$ than for $[Pd(H_2O)_4]^{2+}$. Under our analytical conditions, the relatively short duration between the metal dissolution and the ESI-MS experiments appears to prevent Pd complexation, either alone or in a mixture with nickel nitrate. In this view, at the present stage of our study, this limitation cannot be overcome by simply extending the time to reach complexation equilibrium. Indeed, $[Pd(H_2O)_4]^{2+}$ aqueous solutions are known to be affected by hydrolysis at pH above 2, resulting in the irreversible formation of hydroxido complexes, polynuclear species or even colloidal species in the time-scale of hours [45,46].

3.1.2. Textural properties and bulk metal composition

Table S1 collects the textural properties of the Ni-Pd/Al_2O_3 catalysts (*i.e.* specific surface area, pore volume and pore size) as inferred from N_2 adsorption/desorption at -196 ºC. As pointed out previously on 5Ni/Al catalysts [30], irrespective of the method used, a slight decline of the specific surface area as compared to the bare γ-Al_2O_3 support (154 m^2g^{-1}) occurs after the impregnation of both metals. However, this decrease seems to be less pronounced for the bimetallic 5Ni-yPd/Al catalysts prepared without or with β-CD (Table S1, entries 4-11 *vs.* 1), while no remarkable evolution of the textural properties occurs for a lower metal content in the 2Ni-0.2Pd/Al catalysts (Table S1, entries 14-15 *vs.* 1).

Also, as indicated in Table S1, the metal loadings measured by ICP for the 5Ni-0.5Pd/Al series are very close to the nominal values regardless of the preparation method, falling into the range 4.43-4.93 wt.% for Ni and 0.38-0.45 wt.% for Pd. Besides, good agreement is observed between the nominal and measured Ni and Pd loadings for the 2Ni-0.2Pd/Al catalysts. Overall, these results confirm that the wet impregnation method allows controlling the desired amount of metal ions on the γ-Al_2O_3 support.

3.1.3. Structural properties

3.1.3.1. Preparation Methods 1 and 2

Figure 4 (patterns c and d) plot the XRD patterns of the 5Ni-yPd/Al catalysts prepared by direct co-impregnation method in the absence of β-CD (M1). For comparison, the XRD patterns of the monometallic catalyst, *i.e.* 5Ni/Al and 5Ni/Al-β-$CD_{0.1}$, are also represented (patterns a and b). The XRD line at 33.8º can be assigned to the (101) reflection of PdO crystallites (JCPDS 43-1024), whereas the line at 43.5º is associated to the (200) reflection of NiO (JCPDS 47-1049). The remaining intense lines are ascribed to γ-Al_2O_3. The figure at the right-hand side shows an expanded plot of the range 30-48º including lines with very low intensities due to the low metal loading. By increasing the Pd content, the reflection line of PdO centered at 33.8º becomes visible. Thus, at the highest Pd loading (1 wt.%), a slightly broader PdO line merges with that of γ-Al_2O_3. Figure 4 (patterns e and f) also plots the XRD patterns of the 5Ni-yPd/Al catalysts prepared by Method 2 encompassing the direct co-impregnation of the Ni and Pd precursors in the presence of β-CD (β-CD/Ni=0.1). Regardless of the Pd loading, the intensity of the NiO lines remains low, whereas the line in the range 33-34º indicates the presence of small PdO crystallites as previously observed for the catalysts prepared by Method 1. This effect becomes more pronounced for the catalyst prepared with the highest Pd loading (*i.e.* 5Ni-1.0Pd/Al-CD_M2). Nevertheless, due to the very low intensity of the NiO and PdO reflections, it is difficult to ascertain the crystallite size by Scherrer equation.

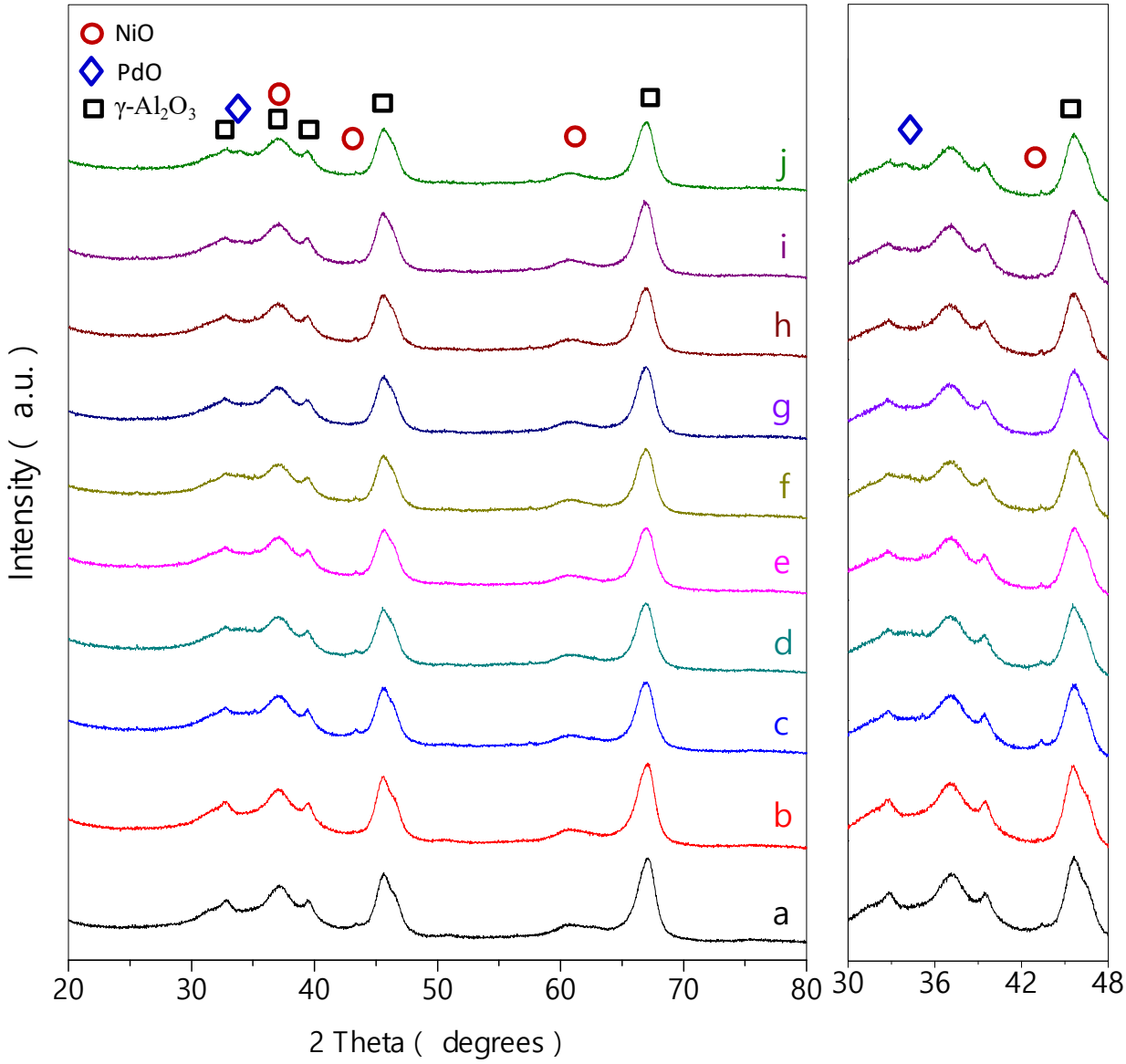

Figure 4. XRD profiles of Ni/Al and Ni-Pd/Al catalysts synthesized both in the absence (Method M1) and in the presence of β-CD (Method M2): a) 5Ni/Al, b) 5Ni/Al-β-$CD_{0.1}$, c) 5Ni-0.5Pd/Al_M1, d) 5Ni-1.0Pd/Al_M1, e) 5Ni-0.5Pd/Al-CD_M2, f) 5Ni-1.0Pd/Al-CD_M2, g) 5Ni-0.5Pd/Al-CD_M3, h) 5Ni-0.5Pd/Al-CD_M4, i) 5Ni-0.5Pd/Al-CD_M5 and j) 5Ni-0.5Pd/Al-CD_M6.

Overall, this body of results could be indicative of a partial segregation between the NiO and PdO phases. However, since the Pd concentration in 5Ni-0.5Pd/Al is very low, it is arduous to conclude at the present stage about any Ni-Pd interaction between both oxides and about the homogeneity of the metal phase.

3.1.3.2. Preparation Methods 3-6

The impact of the impregnation method on the NiO and PdO phases over γ-Al_2O_3 was further investigated. Figure 4 (patterns g-j) shows the XRD patterns of the bimetallic catalysts prepared by Methods 3-6 in the presence of β-CD with the general formulation 5Ni-0.5Pd. The way of introducing β-CD during the catalyst preparation affects to a certain extent the structural organization of the Ni and Pd phases over γ-Al_2O_3. Indeed, slight differences in the reflection lines for NiO (2-theta = 43.5º) can be observed between the different catalysts. Thus, the catalyst prepared by Method 3 shows a less intense line at 43.5º, suggesting that NiO might be better dispersed over this catalyst by shortening the contact time of the Pd precursor. Likewise, only a little change is observed in the region of the (101) reflection of PdO at 33.8º in patterns g-i, whereas this line becomes more visible and defined for the catalyst prepared by Method 6 (pattern j), indicating the presence of PdO nanoparticles with a higher crystallinity. As pointed out above, the latter catalyst was synthesized using a sequential wet impregnation protocol (first Ni with β-CD, then Pd with β-CD with an intermediate calcination step at 400 °C under air). In light of the aforementioned observations, β-CD addition to palladium nitrate during the second impregnation step of 5Ni/Al-β-$CD_{0.1}$ appears to exert a slight detrimental effect on the dispersion of PdO nanoparticles.

In the case of low-metal Ni-Pd/Al catalysts, no major conclusion can be drawn from the XRD patterns on the effect of Method 4 on the metal dispersion due to very low Ni and Pd content (2 wt.% and 0.2 wt.%, respectively) (Figure S3).

3.1.4. Reducibility of the catalysts

3.1.4.1. Preparation Methods 1 and 2

H_2-TPR was used to assess the reducibility of the nickel and palladium oxide phases in the 5Ni-yPd/Al (y = 0.5 or 1) catalysts synthesized by direct co-impregnation both in the absence (Method 1) and in the presence of β-CD (β-CD/Ni=0.1) (Method 2). Figure 5 plots the reduction

profiles of the different catalysts, whereas Table 1 lists the resulting data both in terms of H_2 consumption and reduction temperatures. For comparison, the reduction of the control monometallic catalysts, *i.e.* 5Ni/Al and 5Ni/Al-β-$CD_{0.1}$, are also presented.

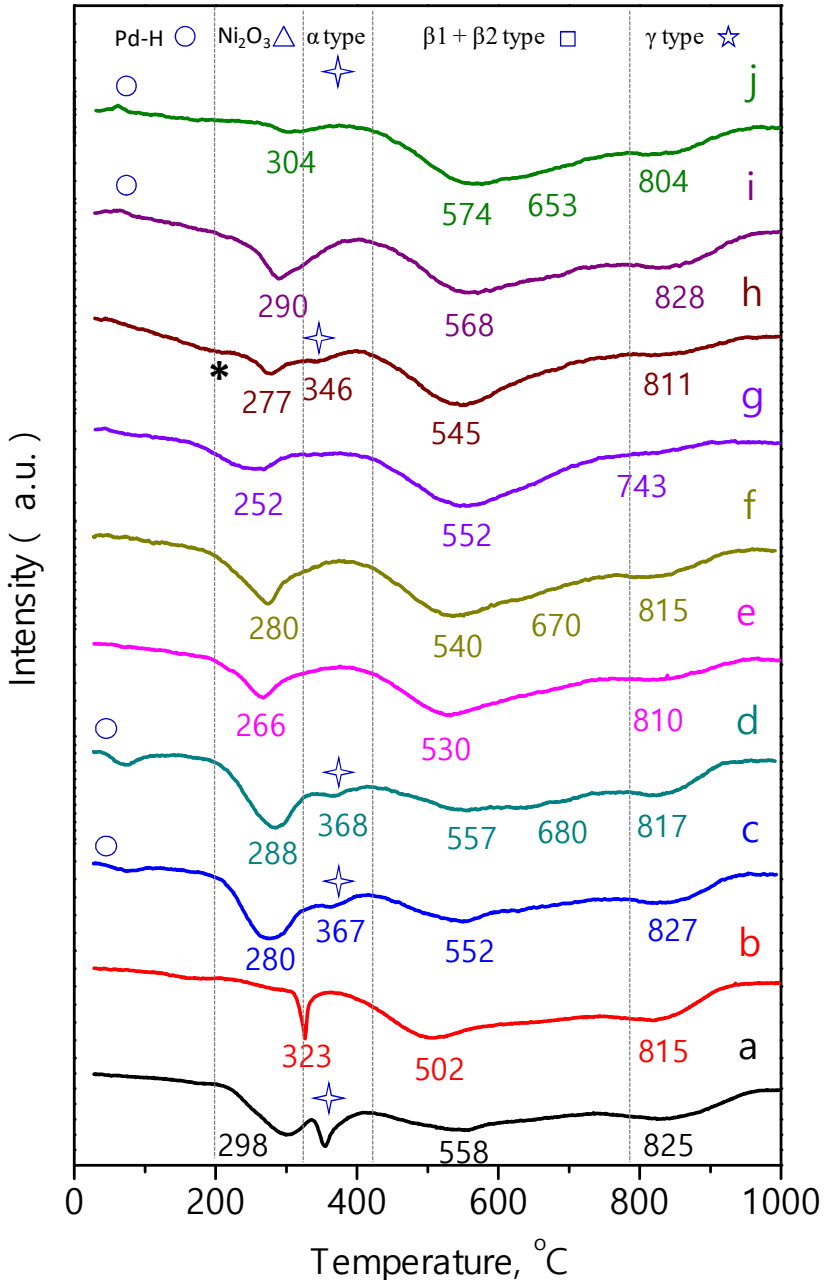

Figure 5. H_2-TPR profiles of 5Ni/Al and 5Ni-Pd/Al catalysts synthesized both in the absence (Method M1) and presence of β-CD (Method M2): a) 5Ni/Al, b) 5Ni/Al-β-$CD_{0.1}$, c) 5Ni-0.5Pd/Al_M1, d) 5Ni-1.0Pd/Al_M1, e) 5Ni-0.5Ni/Al-CD_M2, f) 5Ni-1.0Pd/Al-CD_M2, g) 5Ni-0.5Pd/Al-CD_M3, h) 5Ni-0.5Pd/Al-CD_M4, i) 5Ni-0.5Pd/Al-CD_M5 and j) 5Ni-0.5Pd/Al-CD_M6.

Table 2. Reducibility and physicochemical properties of bimetallic Ni-Pd catalysts synthesized with and without β-CD by different methods

Entry	Catalyst	Total H_2 consum. $\mu mol.g^{-1}$ [a]	Red^n T (°C) Surf Ni^{2+} [b]	%Red^n Ni_2O_3 [c]	%Red^n Bulk Ni^{2+} [d]	%Red^n Surf Ni^{2+} [e]	%Red^n $NiAl_2O_4$ [f]	Dispersion (%D) [g]	Metal Surf. Area, A_m ($m^2.g_{metal}^{-1}$) [h]	Particle size, S_m (nm) [i]
1	2Ni/Al	330 (97)	-	-	38	-	62	13.5	90	7.5
2	2Ni/Al-β-$CD_{0.1}$	266 (89)	-	-	16	-	84	16.2	108	6.2
3	2Ni-0.2Pd/Al_M1	293 (86)	500-700	-	43	30	26	11.3	73	9.1
4	2Ni-0.2Pd/Al-CD_M4	150 (44)	523	-	19	47	34	15.6	101	6.6
5	5Ni/Al	809 (94)	558	16	13	49	22	14.0	95	7.1
6	5Ni/Al-β-$CD_{0.1}$	674 (79)	502	-	6.7	70	23	19.0	133	5.1
7	5Ni-0.5Pd/Al_M1	767 (90)	552	26	7	53	14	9.8	63	10.5
8	5Ni-1.0Pd/Al_M1	692 (81)	557	21	9	58	12	9.4	61	10.9
9	5Ni-0.5Pd/Al-CD_M2	633 (74)	530	18	-	68	14	11.0	71	9.3
10	5Ni-1.0Pd/Al-CD_M2	553 (65)	540	27	-	70	3.4	10.7	67	9.7
11	5Ni-0.5Pd/Al-CD_M3	609 (71)	552	14	-	78	7.9	17.6	114	5.8
12	5Ni-0.5Pd/Al-CD_M4	562 (66)	545	12	7	72	8.4	18.5	119	5.5
13	5Ni-0.5Pd/Al-CD_M5	647 (75)	568	18	-	65	17	13.1	85	7.8
14	5Ni-0.5Pd/Al-CD_M6	584 (68)	574	2.8	-	80	17	12.7	82	8.1

[a] Calculated by integrating the area under the H_2-TPR signal from 150 °C to 1000 °C using Autochem II 2920 software. The numbers in brackets represent the total reduction percentage with respect to the theoretical H_2 consumption calculated on the basis of nominal Ni wt.% loading

[b] Calculated from peak maxima from in the temperature range 400-700 °C

[c] Calculated by dividing the integrated area in the temperature range 150-300 °C by the total H_2 consumption

[d] Calculated by dividing the integrated area in the temperature range 300-450 °C by the total H_2 consumption

[e] Calculated by dividing the integrated area in the temperature range 450-750 °C by the total H_2 consumption

[f] Calculated by dividing the integrated area in the temperature range 750-1000 °C by the total H_2 consumption

[g] Calculated from the CO uptake using equation: (V_{chem}*S.F.*M.W.) / (c/100) *100; V_{chem} is the amount of CO uptake ($mol.g^{-1}$), S.F. is the stoichiometric factor (Metal/CO=2), M.W. is the atomic weight of supported metals and c is the metal loading (wt.%) for Ni and Pd.

[h] Calculated from the equation: (V_{chem}*N_A.*S.F.*σ_m.*10^{-18}) / c *100; where N_A is the Avogadro number and σ_m is cross section area of Ni (0.0649 nm^2) and Pd (0.0787 nm^2)

[i] Mean Ni particle size calculated from the equation: 60c / (A_m*ρ); where A_m is the metal surface area per gram catalyst and ρ is density of Ni (8.9 $g.cm^{-3}$) and Pd (12.0 gcm^{-3}).

Without β-CD addition to the impregnation solution, the H_2-TPR profiles of 5Ni-0.5Pd/Al_M1 and 5Ni-1.0Pd/Al_M1 (Figure 5, profiles c and d) exhibit four main bands that can be assigned to the reduction of four nickel oxide species, namely: (1) Ni_2O_3 centered at *ca.* 290 °C [47-49], (2) bulk NiO centered at *ca*. 370 °C (α-type) [50-52], (3) surface Ni oxides interacting with γ-Al_2O_3 in the range 450-700 °C (β_1+β_2-type), and (4) hard-to-reduce bulk $NiAl_2O_4$ spinel at T > 700°C (γ-type) [25,53-55]. The reduction behavior of these species evolves gradually upon Pd addition, with the total H_2 consumption for NiO reduction decreasing from 809 μmol.g^{-1} for 5Ni/Al to 692 μmol.g^{-1} for 5Ni-1.0Pd/Al_M1 (Table 2, entries 5 and 8). Significant changes are also observed in the high-temperature region upon Pd addition, inhibiting the formation of undesired nickel aluminates from 22% for 5Ni/Al to 14% and 12% for 5Ni-0.5Pd/Al_M1 and 5Ni-1Pd/Al_M1, respectively (Table 2, entries 5, 7 and 8).

When β-CD is directly introduced to the co-impregnation solution containing both the Ni and Pd salts (Method 2), regardless of the Pd content, the reduction temperature of surface nickel oxide species present on the final catalyst becomes significantly affected. For example, using 5Ni-yPd/Al (y = 0.5), the reduction temperature decreases from 552 °C for Method 1 to 530 °C for Method 2 (Table 2, entries 9 *vs.* 7), reflecting a higher reducibility of Ni surface species in 5Ni-0.5Pd/Al-CD_M2. A similar trend is obtained at the highest Pd content (y = 1) with a decrease in temperature ranging from 557 °C to 540 °C (Table 2, entries 10 *vs.* 8). Besides, by using β-CD, the relative proportion of surface NiO species increases to about 68-70% at the expense of bulk NiO (α-type) and nickel aluminates species (Table 2, entries 9 and 10). However, note that this reduction behavior is also observed, even to a larger extent, for the monometallic 5Ni/Al-β-$CD_{0.1}$, showing a marked downward shift in the H_2 consumption corresponding to surface NiO (β_1+β_2 type) species (Table 2 entries 6 *vs.* 5).

Additional information on Pd species can be obtained from the H_2-TPR profiles. For instance, subtle reduction bands ascribed to Pd-H species appear in the range 50-80 °C (Method 1). Nonetheless, these bands appear to have vanished or shifted to lower temperatures for the catalysts

synthesized by Method 2. To gain more insight into the PdO_x reduction behavior and hydride formation, the H_2-TPR profiles were measured for the 5Ni-yPd/Al (y = 0.5 or 1) catalysts prepared by Methods 1 and 2 starting at cryogenic conditions (from -60 ºC to 1000 ºC) (Figure S4, Table S2). In all cases, the H_2-TPR profiles can be divided into two regions: (1) a low-temperature region (from -60 ºC to 290 ºC) being ascribed to PdO_x and Ni_2O_3 reduction, and (2) a high-temperature region (from 290 ºC to 1000 ºC) being ascribed to the reduction of NiO species (*i.e.* α, β_1+β_2 and γ types). In particular, the reduction profile for 5Ni-0.5Pd/Al_M1 shows two bands centered at -12 ºC and 8 ºC (Figure S4, profile a) that can be attributed to large PdO_x crystallites and PdO_x species with weak interaction with NiO. The small positive band at *ca*. 50 ºC can be ascribed to H_2 release from Pd hydride (Pd-H) species [56]. An even more complex low-temperature reduction pattern appears at higher Pd loadings (1 wt.%). Indeed, the reduction of 5Ni-1Pd/Al_M1 exhibits three low-temperature reduction bands (Figure S4, profile c,): (1) two first bands centered at 13 ºC and 27 ºC that can be attributed to the reduction of free PdO_x crystallites (without any interaction with NiO or γ-Al_2O_3) and PdO_x interacting with NiO, respectively, and (2) a third band centered at 52 ºC that can be attributed to the reduction of small PdO_x crystallites in strong contact with Al_2O_3.

The use of β-CD also impacts the PdO_x reduction profile. Indeed, profile b shows two bands centered at 7 ºC and 30 ºC with similar intensity, which could indicate the formation of homogeneous crystallite sizes of both free PdO_x and PdO_x interacting with NiO. Furthermore, the catalyst synthesized with the highest Pd loading (Figure S4, profile d) displays a PdO_x reduction profile with two close and intense bands centered at 21 ºC and 30 ºC, suggesting a more homogeneous reduction pattern of both species with no reducible species at high temperature.

Overall, this body of results highlight that the addition of Pd to NiO/Al_2O_3 enhances the reduction of surface NiO species and minimizes the formation of nickel aluminates, while β-CD addition to bimetallic xNi-yPd/Al by Method 2 further promotes this phenomenon. In terms of reducibility, the addition of small Pd amounts facilitates the reduction of NiO species, leading to

narrowly distributed and smaller Ni particles. Moreover, higher Pd loadings lead to a surface enrichment by Pd and thereby to less exposed Ni species (Table S2, entries 1 and 3). Irrespective of the method (*i.e.* Method 1 and 2), this observation is in agreement with the H_2 consumption corresponding to PdO_x and NiO species (Table 2, Table S2).

3.1.4.2. Preparation Methods 3-6

Figure 5 also plots the H_2-TPR profiles of 5Ni-0.5Pd synthesized by methods 3-6 corresponding to different ways to introduce β-CD as additive during Ni and Pd impregnation (β-CD/Ni=0.1) (profiles g-j). As can be observed, the preparation method exerts a significant impact on the distribution and reducibility of the different Ni species present in the bimetallic catalysts. The catalyst prepared using Method 3 by premixing the Ni salt with β-CD before Pd addition shows a reduction profile characterized by three main bands ascribed to Ni_2O_3 (252 °C), surface NiO (552 °C) and $NiAl_2O_4$ (743 °C) species (profile g). A similar profile is observed when β-CD is pre-added to the Al_2O_3 support (Method 4), displaying only slight differences in the average temperature of the bands and in the relative contributions of the components (profile h). Notwithstanding this fact, it can be noticed that for 5 Ni-0.5Pd/Al-CD_M4, a small hump is visible at ca. 185 °C (represented as a black star), which can be ascribed to the reduction of PdO in strong interaction with Ni surface [57]. In addition, a small peak corresponding to NiO (α-type) reduction is also observed on the same profile. When examining the H_2 consumption, we observe that both methods give rise to higher levels of surface NiO species (β_1+β_2 type). Their proportion can be estimated to *ca*. 78% for 5Ni-0.5Pd/Al-CD_M3 and 72% for 5Ni-0.5Pd/Al-CD_M4 (Table 2 entries 11 and 12). Interestingly, both methods discourage to an important extent the formation of nickel aluminate species (γ-type), decreasing to a percentage about 8%. However, note that for the catalyst prepared by Method 4, the reduction of surface Ni species occurs more easily, as suggested by the slightly lower average temperature of its corresponding band (545 °C instead of 552 °C).

The catalysts prepared by sequential impregnation either in the absence (Method 5) or presence (Method 6) of β-CD (Table 2 entries 13 and 14; Figure 5 profiles i and j) show a higher proportion of nickel aluminates (17%) compared to the catalysts prepared by Methods 3 and 4 (7.9% and 8.4%, respectively) (Table 2, entries 11 and 12). Note that the former percentage (17%) is similar to that measured on the control monometallic catalyst (23%) (Table 2, entry 6). This observation can be explained by the fact that Pd deposition occurs on the calcined NiO/Al_2O_3 catalyst, which was synthesized before Pd impregnation, where nickel aluminates were already present. In terms of Ni_2O_3 and surface NiO (β_1+β_2 type) species, 5Ni-0.5Pd/Al-CD_M5 exhibits a similar reduction percentage for both species compared to 5Ni-0.5Pd/Al-CD_M2 (Table 2, entries 13 and 9). In contrast, 5Ni-0.5Pd/Al-CD_M6 displays a lower proportion of Ni_2O_3 and more surface NiO species, even if slightly less reducible (Table 2, entry 14). As a matter of fact, the reduction profile of the latter catalyst (Figure 5, profile j) reveals that the reduction temperature of surface NiO species is slightly shifted towards higher temperatures, encompassing the formation of β_2 species at 653 ºC covering 80% of the surface NiO species. From these findings, it appears that the use of β-CD during the second impregnation step can help restructuring the as-formed Ni species on Al_2O_3. This behavior could be related to a role of β-CD as complexing agent for Ni, breaking up part of bulk NiO particles on Al_2O_3 and redistributing or rearranging it towards surface NiO species (β_1+β_2 type). Noteworthy, similar effects were reported during the regeneration of spent Al_2O_3-supported metal catalysts by chemical pretreatment using chelating agents (*e.g.*, citric acid, glycolic acid) followed by calcination under air [58].

Turning now our attention into low-Ni-Pd bimetallic catalysts, the addition of 0.2 wt.% Pd to 2Ni/Al in the absence of β-CD (Method 1) leads to a 30% reduction percentage of surface NiO species together with slight increase of bulk NiO species (38% for 2Ni/Al *vs.* 43% for 2Ni-0.2Pd/Al_M1) and less nickel aluminate species (62% for 2Ni/Al *vs*. 26% for 2Ni-0.2Pd/Al_M1) (Table 2, entries 1 and 3; Figure S5 profiles a and c). The extension of Method 4 to low-Ni-Pd bimetallic catalysts results in a dramatic increase of surface Ni species ranging from 30% for 2Ni-

0.2Pd/Al_M1 to 47% for 2Ni-0.2Pd/Al-CD_M4 at the expense bulk NiO, the latter decreasing from 43% to 19% (Table 2, entries 3 and 4; Figure S5 profiles c and d). Overall, the reduction behavior of low-Ni-Pd catalyst prepared by Method 4 is fully consistent with the reduction behavior of 5Ni-0.5Pd/Al-CD_M4, also prepared by pre-adsorbing β-CD on γ-Al_2O_3.

3.1.5. Metal dispersion and average particle size

CO chemisorption was further conducted on the reduced catalysts to measure the metal dispersion, metal surface area, and average particle size. The results are summarized in Table 2. As a rule, β-CD addition results in an increase of the metal dispersion and surface area, and consequently in a decrease of the average particle size. This effect is observed not only for the monometallic catalysts with 2 wt.% and 5 wt.% Ni loading, but also for the bimetallic Ni-Pd catalysts, even though the effect of β-CD on the metal dispersion depends on the preparation method.

As can be observed, without β-CD, the direct co-impregnation of Ni and Pd (Method 1) results in larger metal particle sizes compared to monometallic Ni catalysts also impregnated without β-CD. As an illustrative example, 5Ni/Al (Table 2, entry 5) shows an average particle size of 7.1 nm (metal dispersion = 14%), which increases to 10.5 nm (metal dispersion = 9.8%) for 5Ni-0.5Pd/Al_M1 (Table 2, entry 7). A similar behavior is observed for the bimetallic catalyst with low Ni loading (Table 2, entries 3 *vs*. 1). In contrast, β-CD addition to the Ni and Pd co-impregnation solution exerts a slightly beneficial effect on the average particle size of 5Ni-0.5Pd/Al-CD_M2 (9.3 nm, metal dispersion = 11%) (Table 2, entry 9). This trend, which is also observed at the highest Pd loading (1.0 wt.%) (Table 2, entries 10 *vs*. 9), provides further indication that palladium nitrate does not interact with β-CD in water, limiting its dispersion capacity in the presence of both Ni and Pd salts.

Methods 3 and 4, encompassing β-CD controlled-addition procedures, impact to a higher extent the metal dispersion of bimetallic Ni-Pd catalysts. As listed in Table 2 (entries 11 and 12), 5Ni-0.5Pd/Al-CD_M3 exhibits a higher metal dispersion with an average particle size estimated

at 5.8 nm (metal dispersion = 18%). Interestingly, the metal dispersion is apparently enhanced for 5Ni-0.5Pd/Al-CD_M4, achieving an average particle size as low as 5.5 nm (metal dispersion = 19%). The results indicate that both the decrease of the contact time of the Pd impregnation process (Method 3) and the simultaneous introduction of the Ni and Pd precursors into the γ-Al_2O_3/β-CD aqueous suspension (Method 4) are key drivers for the metal dispersion over γ-Al_2O_3. As already pointed out in the ESI-MS experiments (Figure 2), palladium nitrate does not form any adduct with β-CD in aqueous solution. As a result, a homogeneous distribution of metal particles with higher metal dispersion is obtained by Method 4. This conclusion can be extended to lower Ni formulations, *i.e.* 2Ni-0.2Pd/Al-CD_M4, exhibiting an average particle size of 6.6 nm (metal dispersion = 16%) as compared to the value of 9.1 nm (metal dispersion = 11%) for 2Ni-0.2Pd/Al_M1 (Table 2, entries 4 and 3).

Finally, the remaining methods applied, *i.e.* M5 and M6, relying on the sequential impregnation of the Pd precursor over NiO/Al_2O_3, can afford an average metal particle size of 7.8 nm (metal dispersion = 13%) and 8.1 nm (metal dispersion = 13%), respectively (Table 2, entries 13 and 14). These average particle sizes lie within the values obtained for Method 2 and Methods 3-4.

The size of Ni and Pd nanoparticles and their location on the Al_2O_3 surface was further investigated by STEM-EELS/EDS. Figures 6 and 7 show representative micrographs for 5Ni-0.5Pd/Al-CD_M4 and 5Ni-0.5Pd/Al_M1. Both catalysts were selected as they exhibited the highest and lowest metal dispersion, respectively. On the one hand, 5Ni-0.5Pd/Al_M4 (Figures 6C-E) shows a homogeneous Ni and Pd distribution, both elements appearing at the same location on the Al_2O_3 surface. In contrast, 5Ni-0.5Pd/Al_M1 (Figure 7C-F) gives rise to more isolated individual Pd nanoparticles with slightly larger sizes surrounding a dense distribution of Ni species interacting with Al_2O_3. The STEM micrographs for both samples confirm a better metal dispersion for the former catalyst. As a matter of fact, the Ni and Pd particle size distribution appears in a narrower range for 5Ni-0.5Pd/Al-CD_M4 with a higher proportion (75%) of particles in the size range 3-6 nm (inset, Figure S7A) whereas the distribution for 5Ni-0.5Pd/Al_M1 ranges from 3 to 10 nm

(inset, Figure S6A). These results, which are in good agreement with the average particle sizes measured from pulse CO chemisorption (Table 2), suggest that β-CD pre-adsorption in Method 4 discourages the direct deposition of the two metal salt precursors on the Al_2O_3 surface during the impregnation procedure, thus generating more nucleation centres with enhanced surface interactions between Ni and Pd elements during calcination and reduction stages.

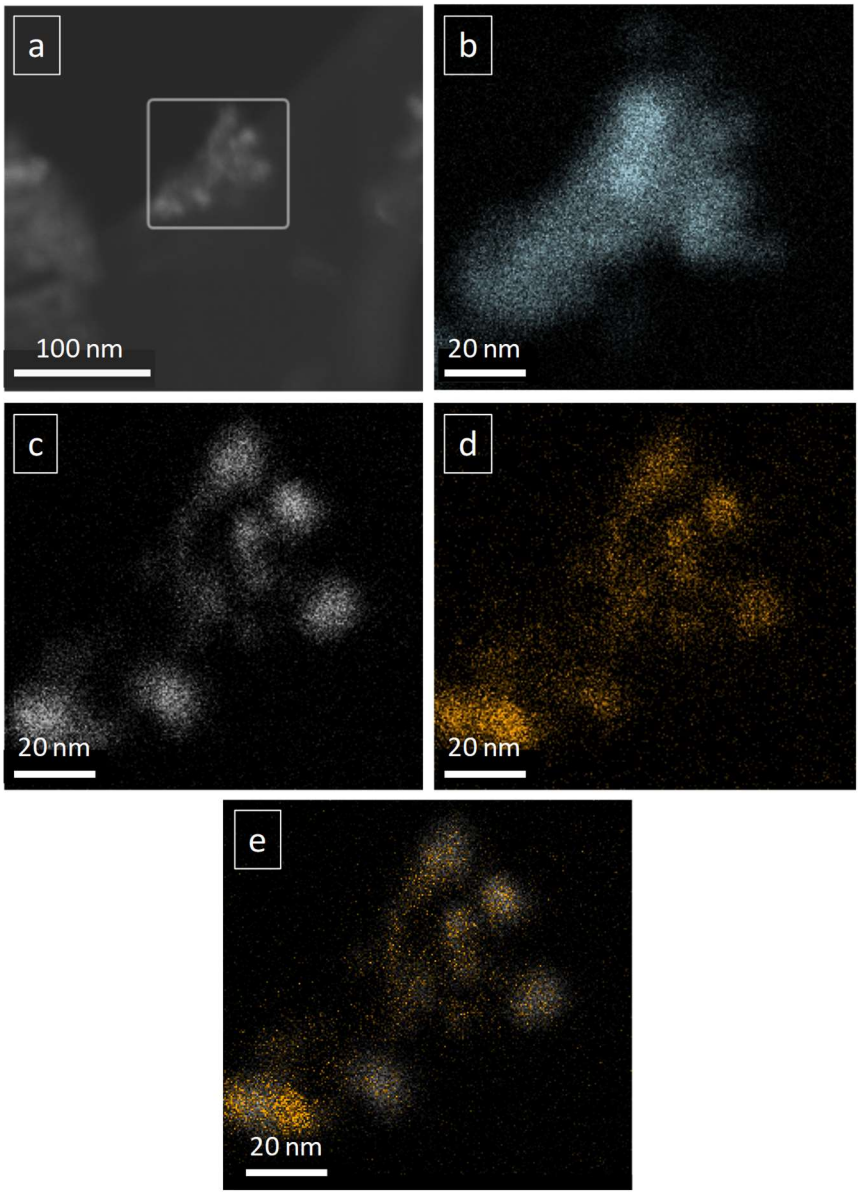

Figure 6. STEM-EELS/EDS micrographs for the catalyst synthesized by Method 4 (5Ni-0.5Pd/Al-CD_M4) during STEM analysis: a) area of EDS map acquisition marked by white rectangle, b) Al K, c) Pd L, d) Ni K, and e) superimposed Pd L and Ni K elements.

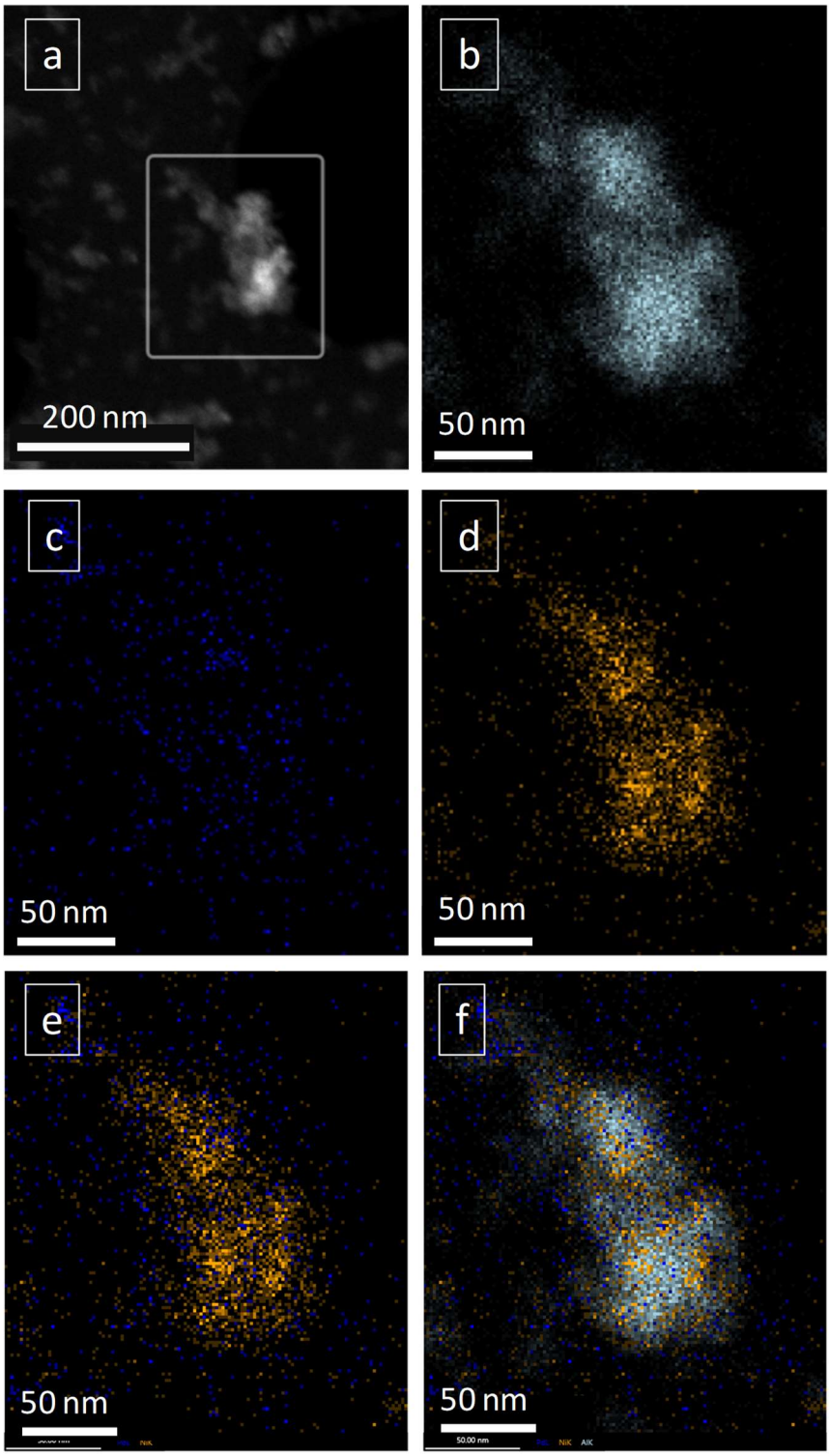

Figure 7. STEM-EELS/EDS micrographs for the catalyst synthesized by Method 1 (5Ni-0.5Pd/Al_M1) during STEM analysis: a) area of EDS map acquisition marked by white rectangle, b) Al K, c) Pd L, d) Ni K, e) superimposed PdL and Ni K elements and f) superimposed Pd L, Ni K and Al K elements.

Table 3. Bulk and surface composition of catalysts synthesized in the absence or presence of β-CD.

Entry	Catalyst	Bulk concentration			Surface concentration					
					Calcined			*Reduced* [a]		
		Ni/Al	Pd/Al	Pd/Ni	Ni/Al	Pd/Al	Pd/Ni	Ni/Al	Pd/Al	Pd/Ni
1	5Ni/Al	0.040	-	-	0.10	-	-	0.051	-	-
2	5Ni-0.5Pd/Al_M1	0.040	0.0019	0.047	0.097	0.011	0.096	0.058	0.0057	0.098
3	5Ni-0.5Pd/Al-CD_M4	0.041	0.0020	0.049	0.14	0.019	0.13	0.068	0.010	0.15

[a] Catalyst pre-reduced under at 580 ^{o}C for 30 min under H_2 flow.

3.2. Metal surface distribution (XPS)

Given the promising metal dispersion achieved on 5Ni-0.5Pd/Al-CD_M4, we characterized in more detail the surface nature and composition of this catalyst by XPS. It is interesting to mention that no band of significant intensity assigned to the C1s core level was observed in the spectrum, confirming the total removal of β-CD during the calcination. For comparison, 5Ni-0.5Pd/Al_M1 and the control monometallic 5Ni/Al were also considered. Figure 8 and Figure 9 plot the XPS spectra of the Ni 2p and Pd 3d core levels for 5Ni-0.5Pd/Al-CD_M4 and 5Ni-0.5Pd/Al_M1 both in their calcined and reduced states, while Figure S8 plots the XPS spectra of the Ni 2p core level for 5Ni/Al. The relative surface concentrations and binding energies determined by XPS are listed in Table 3 and Table S3, respectively.

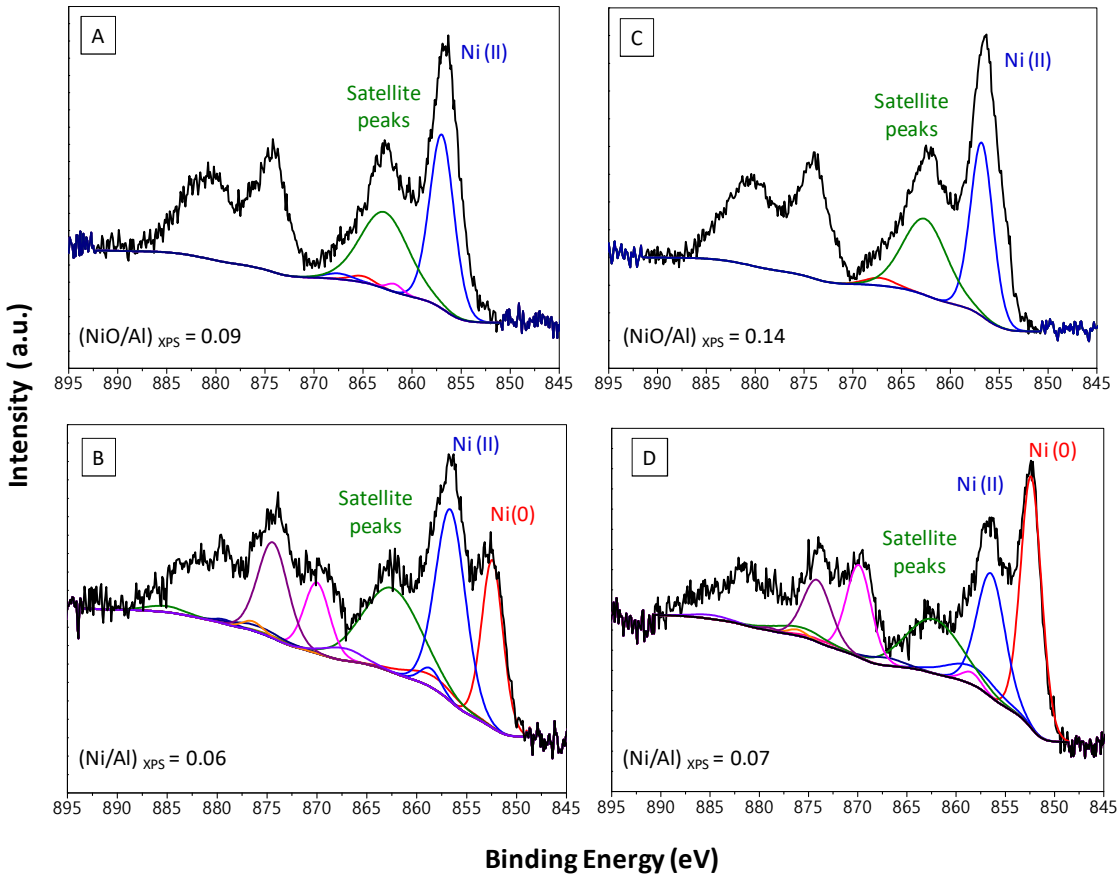

Figure 8. XP spectra for 5Ni-0.5Pd/Al_M1 (A & B) and 5Ni-0.5Pd/Al-CD_M4 (C & D) in calcined and reduced states, respectively, for the Ni 2p core level. The samples were pre-reduced at 580 ºC for 30 min under H_2 flow before XP analysis.

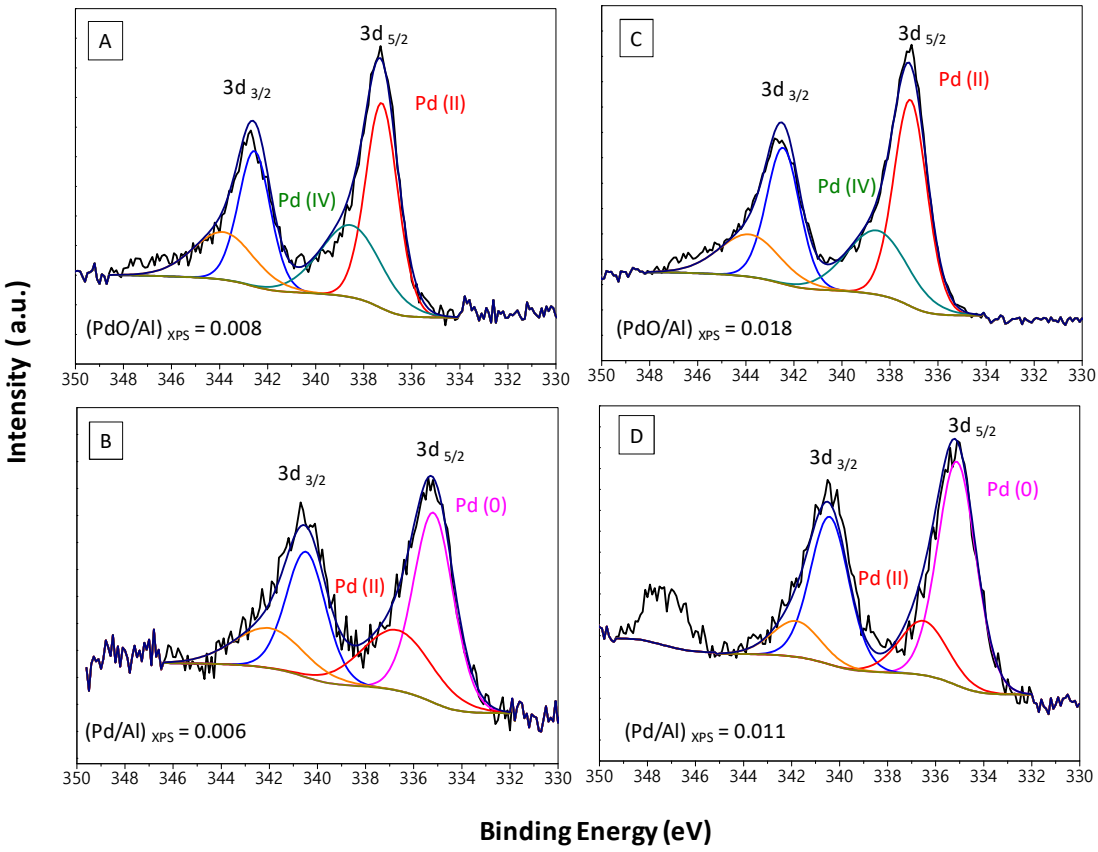

Figure 9. XP spectra for 5Ni-0.5Pd/Al_M1 (A & B) and 5Ni-0.5Pd/Al-CD_M4 (C & D) in calcined and reduced state, respectively, for the Pd 3d core level. The samples were pre-reduced at 580 °C for 30 min under H_2 flow before XP analysis.

When examining the monometallic 5Ni/Al catalyst prepared without β-CD, the XPS spectrum of the Ni 2p region exhibits two main bands centered at 856.5 eV and ~862 eV that are indicative of the Ni^{2+} state and shake-up satellite bands belonging to both NiO and Ni_2O_3, respectively [59,60]. An additional band is observed at 852.2 eV for the *in situ* reduced catalyst (Table S3 entry 1, Figure S8B), which can be attributed to reduced Ni (Ni^0) [61]. The Ni $2p_{3/2}$ XP spectra of 5Ni-0.5Pd/Al_M1 (Figure 8A,B) and 5Ni-0.5Pd/Al-CD_M4 (Figure 8C,D) display a band at 856.3 eV assigned to NiO in the calcined state and a band attributed to Ni^0 at 852.4 eV in the reduced state (Table S3, entries 2 and 3). Interestingly, upon Pd doping even in small amounts, the density of surface Ni species is enhanced after reduction compared to the bulk values (Ni/Al = 0.058 for 5Ni-0.5Pd/Al_M1 *vs.* Ni/Al = 0.040 for 5Ni/Al) (Table 3, entry 2 *vs.* entry 1). This phenomenon

becomes much more pronounced in the presence of β-CD with a percentage increase of about 33% (Ni/Al = 0.068 for 5Ni-0.5Pd/Al-CD_M4 *vs.* Ni/Al = 0.051 for 5Ni/Al) (Table 3, entry 3 *vs.* entry 1).

Turning now our attention into the Pd 3d XPS spectra, both bimetallic catalysts display two major $3d_{5/2}$ and $3d_{3/2}$ spin-orbit bands in the calcined state centered at 337.3/342.6 eV for 5Ni-0.5Pd/Al_M1 (Figure 9A) and 337.1/342.8 eV for 5Ni-0.5Pd/Al-CD_M4 (Figure 9C). These BEs are indicative of $Pd^{II}O$ species on the catalyst surface [62,63], while the additional band appearing after deconvolution at 338.6 eV (Pd $3d_{5/2}$) might be attributed to $Pd^{IV}O_2$ species [64-66]. After *in situ* reduction, the most intense Pd $3d_{3/2}$ and Pd $3d_{3/2}$ lines for both catalysts show BEs at ~335 eV and 340 eV, which are both characteristic of a dominant presence of reduced Pd^0 [67,68]. However, a careful examination of the spectra reflects slightly lower BEs (by *ca.* 0.2 eV) for Ni-0.5Pd/Al-CD_M4 (Table S3, entry 3) compared to 5Ni-0.5Pd/Al_M1 (Table S3, entry 2). This difference suggests a slightly higher extent of reduction to metallic Pd by H_2 for the former catalyst, presumably due to a weaker metal-support interaction. This observation is also consistent with a Pd surface enrichment, as supported by the Pd/Ni atomic ratios from XPS analysis. Indeed, the surface concentrations measured for the calcined 5Ni-0.5Pd/Al-CD_M4 indicate a much higher density of Pd species on the catalyst surface compared to 5Ni-0.5Pd/Al_M1 (Pd^{II}/Al = 0.019 for 5Ni-0.5Pd/Al-CD_M4 *vs.* Pd^{II}/Al = 0.011 for 5Ni-0.5Pd/Al_M1, Table 3 entry 3 vs. entry 2). A similar difference is observed for the catalysts after reduction, showing also a higher surface concentration of Pd species for the catalyst synthesized by Method 4 (Pd/Al = 0.010 for 5Ni-0.5Pd/Al-CD_M4 *vs.* Pd/Al = 0.0057 for 5Ni-0.5Pd/Al_M1, Table 3 entry 3 *vs.* entry 2). In addition, the hypothesis of surface Pd segregation over bimetallic Ni-Pd solid-solution nanoparticles does not appear compatible with our XPS results. Indeed, no significant positive shift of the Pd $3d_{5/2}$ BE indicative of possible alloying with Ni is observed. This observation differs from what is classically observed by XPS on Ni-Pd alloys, displaying higher BEs than the BE of pure Pd^0 due to the existence of $Pd^{\delta+}$ species generated by charge transfer from Pd to Ni [69].

3.3. Catalytic results

3.3.1.1. Preparation Methods 1 and 2

Figure 10 plots the performance of the xNi-yPd/Al catalysts for 1-octanol amination with NH_3 at 160 ºC for 4 h, while Table S4 lists the results obtained. For comparison, the results obtained with the pristine Al_2O_3 and monometallic catalysts are also included.

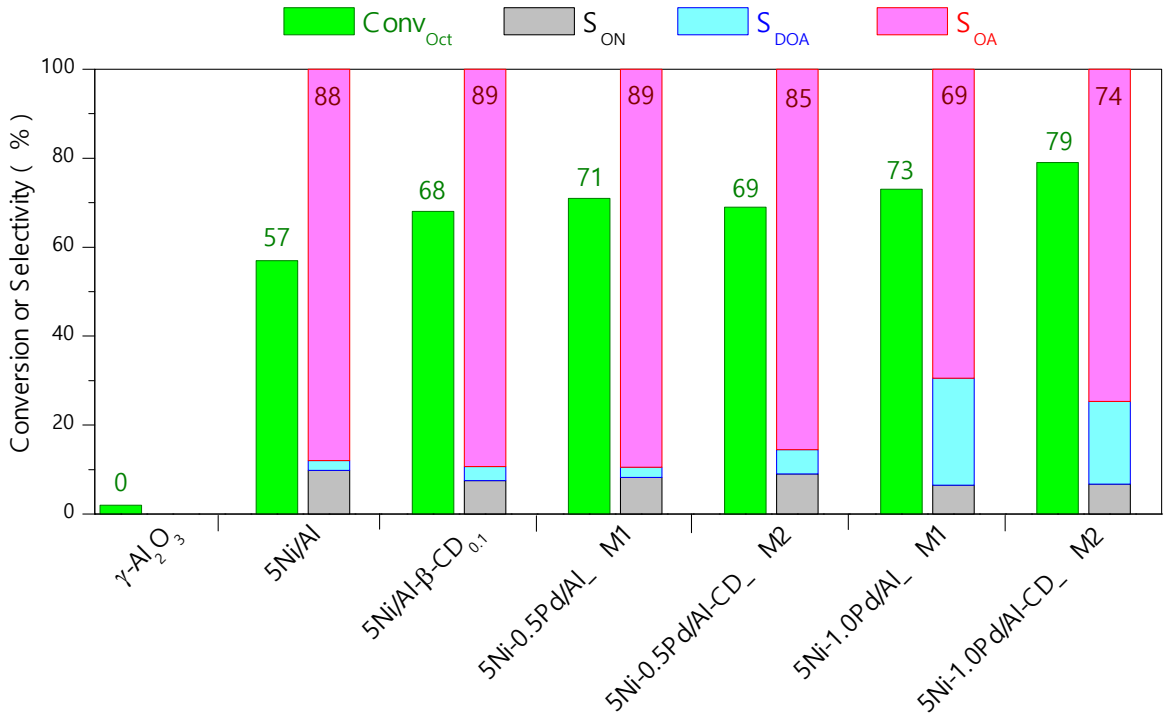

Figure 10. Performance of Ni-Pd/Al catalysts synthesized by Methods 1 and 2 in the amination reaction of 1-octanol with ammonia. The numbers in the graph indicate the 1-octanol conversion and selectivity to different N-products. *Reaction conditions: 1-octanol- 1.3 mmol, NH_3- 7 bar, T- 160 ºC, Time- 4 h, Cat- 60 mg, Solvent- 3 mL o-xylene, rpm- 600.*

At higher Ni loading (5 wt.% Ni), 5Ni/Al shows 57% 1-octanol conversion and 88% OA selectivity. A remarkable enhancement of the activity is observed when 0.5 wt.% Pd is added to 5Ni/Al by co-impregnation with the 1-octanol conversion increasing from 57% to 71% at constant OA selectivity (~90%) (Table S4, entries 6 and 8). A further increase of the Pd loading to 1 wt.% decreases the OA selectivity to 69% at the expense of DOA (24% selectivity) while keeping the 1-octanol conversion almost unchanged (71-73%). This strong decline in the OA selectivity can

be explained by a surface enrichment by Pd crystallites over Al_2O_3. As inferred from the H_2-TPR profiles (Figure S4 profile c, Table S2 entry 3), the H_2 consumption by NiO species decreases drastically from 736 μmol.g^{-1} for 5Ni-0.5Pd/Al_M1 to 511 μmol.g^{-1} for 5Ni-1.0Pd/Al_M1. This observation indicates that most of the Al_2O_3 surface is covered by small Pd crystallites interacting with Al_2O_3, which is in line with the third band appearing at 52 °C in Figure S4 (profile c). Noteworthy, this third band is only visible at high Pd loading (1.0 wt.%).

β-CD addition to the co-impregnation solution to generate 5Ni-0.5Pd/Al-CD_M2 does not affect to an important extent the catalytic properties, achieving 69% 1-octanol conversion and 85% OA selectivity, which are both very similar to the values obtained for 5Ni-0.5Pd/Al_M1 (without β-CD). Interestingly, the catalytic performance of 5Ni-0.5Pd/Al-CD_M2 is also close to that of the parent 5Ni/Al-β-$CD_{0.1}$ synthesized in the presence of β-CD under similar impregnation conditions (*i.e.* water volume, alumina weight), but with no Pd. The 1-octanol reactivity increases slightly upon Pd addition (1%) with a 1-octanol conversion reaching 79%, but with less OA (75%) at the expense of DOA (19%). (Figure 10, Table S4 entries 7, 9 and 11). These results indicate that β-CD addition to the bimetallic solution provides no significant benefit on the final catalytic properties, and that this behavior greatly differs from that prevailing in the monometallic catalysts [30]. We attribute this observation to the lack of direct interaction between Pd and β-CD (either in its free form or complexed with the Ni precursor) in the aqueous co-impregnating solution, resulting in independent units that are transported to the Al_2O_3 surface during impregnation. These units are expected to favor the nucleation and growth of phase-separated metal oxide clusters (NiO and PdO) after solvent evaporation and thermal activation without affecting substantially the number of contact points between both metals.

3.3.1.2. Preparation Methods 3-6

We further explored the effect of the preparation method on the performance of 5Ni-0.5Pd/Al catalysts with low Pd loadings. Figure 11 and Table S4 compile the results obtained. The catalysts

prepared by Methods 3 and 4 display the highest activity, affording 93% and 90% 1-octanol conversion and 71% and 79% OA selectivity, respectively, after reaction at 160 ºC for 4 h. In particular, 5Ni-0.5Pd/Al-CD_M3 shows higher DOA selectivity (22%), while 5Ni-0.5Pd/Al-CD_M4 only shows 15% DOA selectivity. The higher OA selectivity of the latter catalyst can be attributed to the lower reduction temperature of surface Ni species (545 ºC *vs* 552 ºC) at comparable percent reduction of surface Ni species (72% *vs* 78 %, Table 2 entries 11 and 12). As pointed out above, the H_2-TPR profiles of both catalysts also exhibit a different reduction behavior (Figure 5, profiles g and h). Indeed, the catalyst synthesized by Method 4 exhibits the highest OA yield (71%) at 90% conversion.

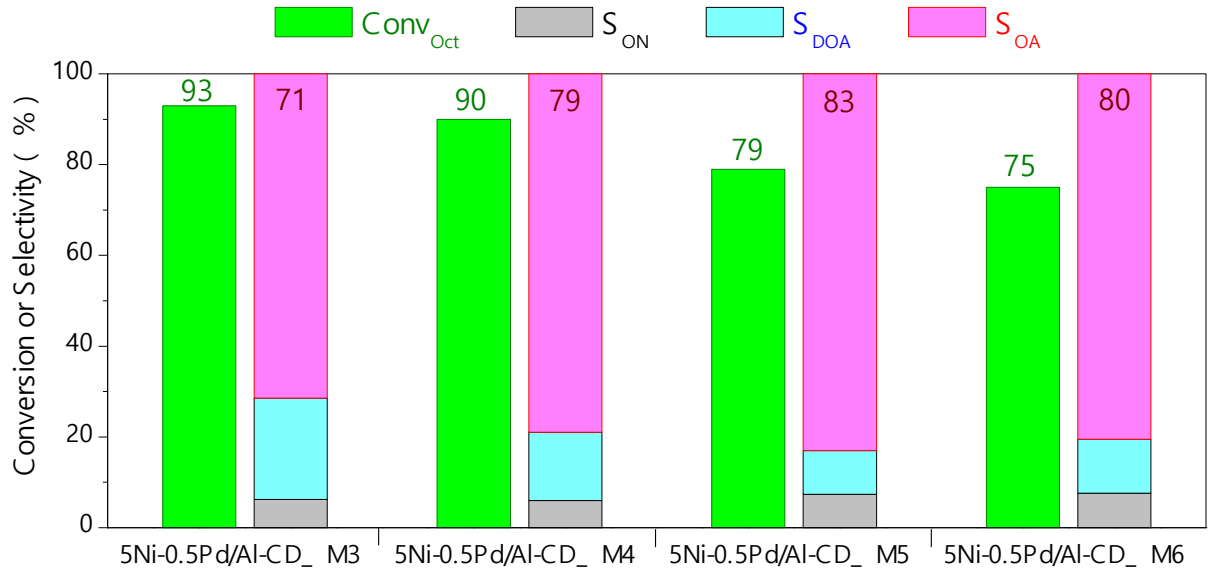

Figure 11. Performance of 5Ni-0.5Pd/Al catalysts synthesized by Methods 3-6 in the amination reaction of 1-octanol with ammonia. The numbers in the graph indicate the 1-octanol conversion and selectivity to different N-products. *Reaction conditions as in Figure 10.*

The catalysts synthesized by sequential impregnation, *i.e.* Methods 5 and 6, exhibit different activities and OA yields (Figure 11 and Table S3 entries 14 and 15). In particular, the catalyst synthesized by Method 5 displays a slightly higher conversion (79%) with 83% OA selectivity. If β-CD interacted with Pd ions during the impregnation step, this would certainly lead to the generation of well-dispersed Pd species over Al_2O_3. However, this is not the case as confirmed by the

ESI-MS experiments (Figure 2). Indeed, β-CD addition during the second impregnation step (Pd) does not provide any beneficial effect. On the contrary, β-CD promotes a decrease of the 1-octanol conversion from 79% for 5Ni-0.5Pd/Al-CD_M5 to 75% for 5Ni-0.5Pd/Al-CD_M6, encompassing a concomitant decline of the OA selectivity from 83% to 81%. The lack of interaction between β-CD and Pd ions is expected to result in a non-useful excess of β-CD on the catalyst, which has to be removed at 400 ºC in air. Knowing that β-CD decomposition is highly exothermic [70,71], it can be suggested that the second calcination step impacts the size and dispersion of surface Ni species, resulting in a lower activity for the catalyst synthesized by Method 6. This idea is consistent with the CO chemisorption data (13% dispersion and 8.1 nm metal particle for 5Ni-0.5Pd/Al-CD_M6 *vs.* 18% dispersion and 5.5 nm for 5Ni-0.5Pd/Al-CD_M4). Besides, when comparing the H_2-TPR profiles of 5Ni-0.5Pd/Al-CD_M5 and 5Ni-0.5Pd/Al-CD_M6 (Figure 5, profiles i and j; Table 2, entries 13 and 14), the latter catalyst exhibits a lower H_2 consumption and a higher proportion of β_2-type NiO species. This behavior might be explained by the presence of large Pd aggregates as evidenced by the formation of Pd-H species, which agrees well with the XRD patterns (Figure 4, profile j).

3.4. Extension of Method 4 to low-metal (Ni and Pd) catalysts

Since the catalyst synthesized by Method 4 clearly displays the best catalytic performance in terms of OA yield, we extended this method to the preparation of catalysts with lower Ni content (*i.e.* 2Ni-0.2Pd/Al) in the presence of β-CD. Our aim here was twofold: (1) to avoid a high metal concentration on the catalyst, and (2) to activate 2Ni/Al, which is typically inactive for amination due to the absence of surface Ni species (β type) [22,23]. Control experiments on monometallic 0.5Pd/Al, 0.5Pd/Al-β-$CD_{0.1}$, 2Ni/Al and 2Ni/Al-β-$CD_{0.1}$ confirm the total inactivity of these catalysts for 1-octanol amination (Figure S9). Opposing these results, 2Ni-0.2Pd/Al_M1 synthesized without β-CD results in 37% 1-octanol conversion with 24% OA yield. The increase of activity

compared to the parent 2Ni/Al can be ascribed to a higher density of surface Ni species with enhanced reducibility induced by Pd. However, the same formulation prepared with β-CD assistance using Method 4 (*i.e.* 2Ni-0.2Pd/Al-CD_M4) affords a clear enhancement of the 1-octanol conversion to 55% with 33% OA yield (Table S4, entry 5). The higher activity obtained for this low-Ni catalyst (2 wt.% Ni) prepared by pre-contacting β-CD on the support can be correlated to its specific characteristics. Indeed, the high density of β-type Ni species (47%) (Table 2, entry 4) combined with a good reducibility at moderate temperatures (T ~450-600°C) should provide a large number of Ni active sites with more points of contact with Pd, enhancing in turn the catalytic activity.

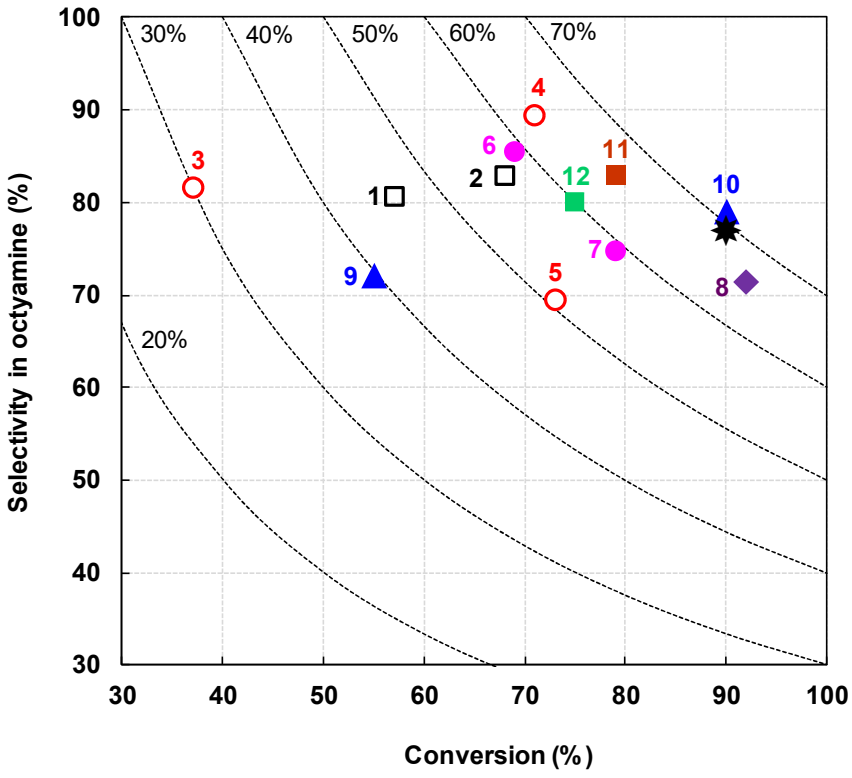

Figure 12. OA selectivity *vs*. 1-octanol conversion for the different catalysts prepared in this study: (1) 5Ni/Al (2) 5Ni/Al-β-$CD_{0.1}$, (3) 2Ni-0.2Pd/Al_M1, (4) 5Ni-0.5Pd/Al_M1, (5) 5Ni-1.0Pd/Al_M1, (6) 5Ni-0.5Pd/Al-CD_M2, (7) 5Ni-1.0Pd/Al-CD_M2, (8) 5Ni-0.5Pd/Al-CD_M3, (9) 2Ni-0.2Pd/Al-CD_M4, (10) 5Ni-0.5Pd/Al-CD_M4, (11) 5Ni-0.5Pd/Al-CD_M5 and (12) 5Ni-0.5Pd/Al-CD_M6. Black star represents the benchmark catalyst (10Ni/θ-Al_2O_3) reported by Shimizu and co-workers [14]. The dashed lines represent the iso-yield curves in OA.

Figure 12 gathers the results obtained in terms of OA selectivity *vs*. 1-octanol conversion for the complete series of monometallic and bimetallic catalysts synthesized by the different methods either without (Method 1), or with β-CD (Methods 2 to 6). The highest OA yield (71%) is achieved for the catalyst synthesized by Method 4 in the presence of β-CD (5Ni-0.5Pd/Al-CD_M4, entry 10) followed by the catalyst synthesized by Method 3 in the absence of β-CD (5Ni-0.5Pd/Al-CD_M3, entry 8) with 64% OA yield. Both catalysts find their place in the top right corner of the plot, whereas the bimetallic catalysts synthesized at lower Ni and Pd loadings (2Ni-0.2Pd) are preferentially located in the middle-left part of the plot. Among the different catalysts, 2Ni-0.2Pd/Al-CD_M4 (entry 9) synthesized in the presence of β-CD exhibits a higher activity compared to 2Ni-0.2Pd/Al_M1 (entry 3).

Further, we compared the catalytic activity of the best bimetallic catalysts prepared in this study against a control monometallic catalyst for 1-octanol amination with NH_3 at 160 ^oC (Figure 12). The bimetallic 5Ni-0.5Pd/Al-CD_M4 exhibits the highest conversion (90%) at a comparable OA selectivity (80-90%) unlike the control 5Ni/Al and 5Ni/Al-β-$CD_{0.1}$. Moreover, higher TON values (90-140) are achieved for the bimetallic catalysts after 4 h reaction compared to the monometallic catalysts (70-80) (Table 4). Also noteworthy, the TONs measured for 5Ni-0.5Pd/Al_M1 and 5Ni-0.5Pd/Al-CD_M4 are higher than the values reported by Shimizu and co-workers over 10Ni/θ-Al_2O_3 (TON= ~85 at 160 ^oC for 13 h) [14]. In other words, by doping very small amount of Pd to the Ni precursor solution for the catalyst synthesized by Method 4, about 67% of Ni can be saved on the final catalyst while keeping a similar 1-octanol conversion (90%) and OA yield (~70%) (Table 4, entries 4 and 5).

Table 4. Comparison of catalytic activity of Ni-Pd/Al and Ni/Al catalysts for the direct amination of 1-octanol with ammonia[a]

Entry	Catalyst	%D[b]	Ni (mol%)	Pd (mol %)	% Oct Conv[c]	% Selectivity[d]					% Yield	TON[e]	CB
						ON	OA	DOA	TOA	DOI	OA		
1	5Ni/Al	14	3.8	-	57	10	88	2.0	0	0	46	84	96
2	5Ni/Al-β-$CD_{0.1}$	19	3.8	-	68	8.0	89	3.0	0	0	56	75	98
3	5Ni-0.5Pd/Al_M1	9.7	3.8	0.21	71	8.2	90	2.3	0	0	55	135	91
4	5Ni-0.5Pd/Al-CD_M4	19	3.8	0.21	90	6.0	79	15	0	0	71	93	101
5	10Ni/θ-Al_2O_3[f]	16	5.0	-	90	-	78	7.7	-	-	70	83	85

[a] Reaction conditions: 1-octanol- 1.3 mmol, NH_3- 7 bar, T- 160 °C, Time- 4 h, Solvent- 3 mL o-xylene, rpm- 600

[b] Dispersion calculated from CO-Pulse chemisorption considering metal/CO, S.F. = 2

[c] Estimated from GC

[d] Normalized selectivity

[e] TON: moles of OA formed per moles of surface Ni at 4 h for entries 1,2 and 5; moles of OA formed per total moles of surface Ni+Pd at 4h for entries 3 and 4

[f] Reaction conditions: 1-octanol- 3 mmol, NH_3- 4 bar, T- 160 °C, Time- 13 h, Solvent -4 mL o-xylene [14]

3.5. Discussion: Genesis of the active Ni-Pd/Al_2O_3 phase by Method 4

The body of results presented above outlines the importance of the preparation method in modifying the surface distribution of Ni and Pd species driven by a subtle interplay of interactions. Indeed, the largest effects in terms of metal dispersion, metal particle size, surface area, percentage of reducible surface Ni species and catalytic activity are observed when β-CD is first put in contact with Al_2O_3 before impregnating the nickel and palladium nitrate salts (Method 4). The suggested mechanism is shown in Figure 13. This pre-contact can lead to the formation of an adsorbed β-CD layer on the Al_2O_3 surface. It is well known that CDs, and most especially native CDs, show affinity for inorganic oxides (*e.g.*, SiO_2 [72],TiO_2 [73] or Al_2O_3 [74]). The adsorption mechanism is usually driven by interactions occurring between the hydroxyl groups of β-CD and the hydroxyl groups on the support surface. Evidence for the affinity of β-CD towards alumina was also given by isothermal adsorption experiments (Figure S10). We observe that the uptake data fit the Langmuir model satisfactorily, while the amount of adsorbed β-CD on the Al_2O_3 surface at saturation is estimated to be 45 μmol g^{-1}, corresponding to a surface density of 0.18 β-CD units/nm^2. Taking into account that the outer diameter of β-CD units is about 1.54 nm, this result seems to indicate that about one third of the alumina surface is occupied by β-CD, with reference to the Langmuir-type adsorption profile (Figure 13a).

When the Ni and Pd salts are impregnated together on the CD-Al_2O_3 suspension, the adsorbed β-CD units are expected to capture preferentially the Ni precursor as compared to the Pd precursor by forming ion-molecule adducts with Ni(II) cations [*i.e.* β-CD-Ni(II)] (Figure 2). These adducts might also act as supramolecular barriers, slowing down the further adsorption of Pd species on the CD-modified Al_2O_3 surface. Noteworthy, such a kinetic effect has been

already reported to explain the divergent complexation behavior of Ni and Pd [42]. Such process may favor the distribution of Pd(II) aqua-complexes in the vicinity of the β-CD-Ni(II) adducts together with the nitrate counterions (Figure 13b). This architecture is expected to be maintained after drying, in line with previous studies (Figure 13c) [30,75].

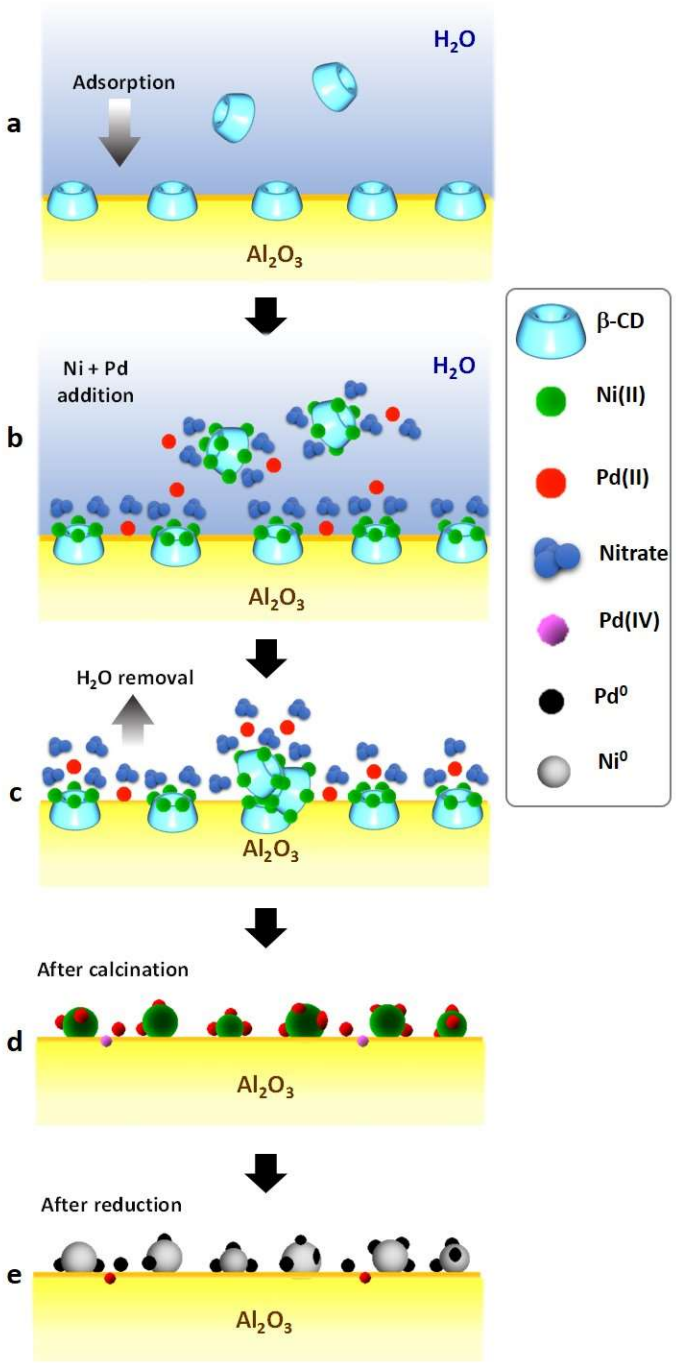

Figure 13. Representative model of interaction of β-CD, Ni and Pd nitrates at different stages for the catalyst prepared by Method 4.

The particular arrangement between Pd-Ni-CD over Al_2O_3 obtained by method M4 impacts the particle size distribution of the metal phase and the Ni and Pd speciation after CD removal by calcination. This can be clearly visualized for 5Ni-0.5Pd/Al-CD_M4. On the one hand, the particle size distribution of the metal phase for this catalyst is much narrower compared to that measured on 5Ni-0.5Pd/Al_M1 (3-6 nm *vs*. 2-10 nm, Figures S6, S7). On the other hand, the XPS measurements clearly point out a higher surface enrichment by Pd compared to Ni after calcination for 5Ni-0.5Pd/Al-CD_M4 and 5Ni-0.5Pd/Al_M1, leading in both cases to higher Pd/Ni surface ratios compared to the bulk ratios (0.15 and 0.098 *vs*. 0.047-0.049), Table 3 entries 2 and 3). This preferential Pd enrichment along with the Ni and Pd superposition observed by STEM-EELS/EDS points out a strong interaction between Pd and Ni on the Al_2O_3 surface, resulting probably in a partial coverage of NiO nanoparticles by PdO_x, as well as in a higher number of contact points between Ni and Pd. This effect becomes more pronounced when β-CD was pre-adsorbed on Al_2O_3 for 5Ni-0.5Pd/Al-CD_M4 (Figure 13d), also resulting in a higher proportion of NiO (β-type) nanoparticles as evidenced by H_2-TPR (Table 2).

The catalyst evolution during the reduction step is strongly impacted by the metal architecture generated after calcination, which is in turn affected by the presence of pre-adsorbed β-CD on Al_2O_3 before impregnation. Overall, 5Ni-0.5Pd/Al-CD_M4 shows smaller average particle sizes for the metal phase compared to 5Ni-0.5Pd/Al_M1 as inferred by CO pulse chemisorption (5.5 nm *vs*. 10.5 nm, Table 2 entries 12 and 7). Besides, the surface enrichment by Pd compared to Ni underlined above for both catalysts after calcination is still visible after reduction (Table 3). Accordingly, we can tentatively propose a partial surface segregation of Pd^0 over Ni^0, which is apparently accentuated for 5Ni-0.5Pd/Al-CD_M4 (Figure 13e). This body of observations illustrates the crucial effect of β-CD in 5Ni-0.5Pd/Al-CD_M4 on pre-shaping the NiO-PdO_x nanoparticles after calcination, which is favourably kept for 5Ni-0.5Pd/Al-CD_M4 after reduction. This specific arrangement between Ni^0 and Pd^0 in 5Ni-0.5Pd/Al-

CD_M4 combined with a higher Ni dispersion results in an enhanced catalytic activity for 1-octanol amination with NH_3 (Figures 10 and 11).

4. Conclusions

We have reported along this paper the preparation of a series of low-Ni (2 or 5 wt.%) Ni-Pd bimetallic catalysts over alumina by different impregnation methods either in the absence or presence of β-CD. The preparation method impacts to an important extent the surface properties of the catalysts, which is driven by the presence of pre-adsorbed β-CD on alumina before impregnating the Ni and Pd precursor solution. This results in a preferential complexation of Ni(II) by the formation of ion-molecule adducts with β-CD as evidenced by ESI-MS, discouraging in turn the further adsorption of Pd(II) on the CD-modified Al_2O_3 surface. This particular arrangement is maintained after drying and conditions to an important extent the particle size distribution of the metal phase, as well as the Ni and Pd speciation (i.e. surface enrichment of Pd compared to Ni) and the reducibility on the calcined catalysts. This general picture is essentially preserved after reduction under a H_2 atmosphere and impacts directly the activity for 1-octanol amination with NH_3 with a conversion up to 90% and an OA yield of 71% at 160 ºC for 4 h (TON = 93). These results place this catalyst among the best ever reported catalysts for amination, but encompassing very low Ni loading and offering a save of 67% of Ni in the reactor compared to benchmark Ni catalysts.

Author Contributions

The manuscript was written through contributions of all authors. All authors have given approval to the final version of the manuscript.

Acknowledgements

This work was supported by the French Agency of Research (ANR) through the SHAPes program (contract 13-CDII-0004-06). The authors also acknowledge the Chevreul Institute (FR 2638), Ministère de l'Enseignement Supérieur et de la Recherche, Region Nord-Pas de Calais and FEDER program for supporting and partially funding this work, as well as the Lille University Computational Center (CRI) for CPU time allocation. The authors would like to express their gratitude to Dr. Eric Leroy from ICMPE-CMTR (UMR 7182 CNRS) and Martine Trentesaux (UCCS, Univ. Lille) for conducting the STEM-EELS/EDS and XPS analyses, respectively. The authors are grateful to Dr. Nicolas Kania (UCCS, Univ. Artois) for his assistance for the H_2-TPR and CO-chemisorption analyses and Laurence Burylo (UCCS, Univ. Lille) for the XRD measurements, as well as to Dr. Joëlle Thuriot (REALCAT, Ecole Centrale Lille) for the ICP analyses. Finally, the authors are grateful to Roquette Frères (Lestrem, France) for the generous gift of β-cyclodextrin.

References

[1] H. A. Wittcoff, B. G. Reuben, J. S. Plotkin, in: Industrial Organic Chemicals, 2nd edition, Wiley, New York, 2004.

[2] S. A. Lawrence, in: Amines: Synthesis, Properties and Applications, Cambridge University Press, New York, 2004.

[3] K. Eller, E. Henkes, R. Rossbacher, H. Höke, in Ulmann's Encyclopedia of Industrial Chemistry, Wiley-VCH, Weinhein, 2002.

[4] M. Pera-Titus, F. Shi, ChemSusChem 7 (2014) 1-4.

[5] G. Guillena, D. J. Ramón, M. Yus, Chem. Rev. 110 (2009) 1611-1641.

[6] S. Bähn, S. Imm, L. Neubert, M. Zhang, H. Neumann, M. Beller, ChemCatChem 3 (2011) 1853-1864.

[7] Q. Yang, Q. Wang, Z. Yu, Chem. Soc. Rev. 44 (2015) 2305-2329.

[8] A. Corma, J. Navas, M. J. Sabater, Chem. Rev. 118 (2018) 1410-1459.

[9] R. G. Rice, E. J. Kohn, Raney, J. Am. Chem. Soc. 77 (1955) 4052-4054.

[10] A. Mehta, A. Thaker, V. Londhe, S. R. Nandan, Appl. Catal. A: Gen. 478 (2014) 241-251

[11] G. A. Vedage, L. A. Emig, H-X. Li, J. N. Armor, US Patent 5 917 092 (1998), to Air Products and Chemicals, Inc.

[12] G. A. Vedage, K. S. Hayes, M. Leeaphon, J. N. Armor, US Patent 5 932769 (1998), to Air Products and Chemicals, Inc.

[13] K-I. Shimizu, K. Kon, W. Onodera, H. Yamazaki, J. N. Kondo, ACS Catal. 3 (2013) 112-117.

[14] K-I. Shimizu, K. Kon, W. Onodera, H. Yamazaki, J. N. Kondo, ACS Catal. 3 (2013) 998-1005.

[15] A. Tomer, Z. Yan, A. Ponchel, M. Pera-Titus, J. Catal. 356 (2017) 133-146.

[16] D. Ruiz, A. Aho, P. Mäki-Arvela, N. Kumar, H. Oliva, D. Y. Murzin, Ind. Eng. Chem. Res. 56 (2017) 12878-12887.

[17] A. Y. K. Leung, K. Hellgardt, K. K. M. Hii, ACS Sustainable Chem. Eng. 6 (2018) 5479-5484.

[18] A. Baiker, J. Kijenski, Catal. Rev. Sci. Eng. 27 (1985) 27, 653-697.

[19] H. Kimura, H. Taniguchi, Appl. Catal. A: Gen. 287 (2005) 191-196.

[20] Y. Li, Q. Li, L. Zhi, M. Zhang, Catal. Lett. 141 (2011) 1635-1642.

[21] J. Sun, X. Jin, F. W. Zhang, W. Hu, J. Liu, R. Li, Catal. Commun. 24 (2012) 30-33.

[22] Y-J. Huang, J. A. Schwarz, J. R. Diehl, J. P. Baltrus, Appl. Catal. 36 (1988) 163-175.

[23] C-W. Hu, C-W. J. Yao, H-Q. Yang, Y. Chen, A-M. Tian, J. Catal. 166 (1997) 1-7.

[24] A. S. Ivanova, E. M. Slavisnskaya, R. V. Gulyaev, V. I. Zaikovskii, O. A. Stonkus, I. G. Danilova, L. M. Plyasova, I. A. Polukhina, A. I. Boronin, Appl. Catal. B: Environ. 97 (2010) 57-71.

[25] A. Zhao, W. Ying, H. Zhang, H. Ma, D. Fang, Catal. Commun. 17 (2012) 34-38.

[26] D. Li, Y. Nakagawa, K. Tomishige, Appl. Catal. A: Gen. 408 (2011) 1-24.

[27] S. Li, J. Gong, Chem. Soc. Rev. 43 (2014) 7345-7256.

[28] F. Liao, T. W. B. Lo, S. C. E. Tsang, ChemCatChem 7 (2015) 1998-2014.

[29] S. De, J. Zhang, R. Luque, N. Yan, Energy Environ. Sci. 9 (2016) 3314-3347.

[30] A. Tomer, F. Wyrwalski, C. Przybylski, J.-F. Paul, E. Monflier, M. Pera-Titus, A. Ponchel, J. Catal. 356 (2017) 111-124.

[31] C. Przybylski, V. Bonnet, Rapid Commun. Mass Spectrom. 27 (2013) 75-87.

[32] C. Przybylski, V. Bonnet, C. Cezard, Phys. Chem. Chem. Phys. 17 (2015) 19288-19305.

[33] K. Nakai, K. Kamura, BELCAT Note, Pulse Chemisorption Measurement, 6th June 2003.

[34] G. Kresse, J. Hafner, Phys. Rev. B: Condens. Matter Mater. Phys. 48(1993) 13115-13118.

[35] G. Kresse, J. Hafner, Phys. Rev. B: Condens. Matter Mater. Phys. 49 (1994) 14251-14269.

[36] G. Kresse, J. Furthmüller, Comput. Mater. Sci. 6 (1996) 15-50.

[37] G. Kresse, J. Furthmüller, Phys. Rev. B: Condens. Matter Mater. Phys. 54 (1996) 11169-11186.

[38] J. P. Perdew, K. Burke, M. Ernzerhof, Phys. Rev. Lett. 77 (1996) 3865-3868.

[39] P. E. Blöchl, Phys. Rev. B: Condens. Matter Mater. Phys. 50 (1994) 17953-17979.

[40] K. Mathew, R. Sundararaman, K. Letchworth-Weaver, T. A. Arias, R. G. Hennig, J. Chem. Phys. 140 (2014) 084106.

[41] K. Mathew, R. G. Hennig, arXiv (2016) [arXiv:1601.03346].

[42] L. Helm, A. E. Merbach, Coord. Chem. Rev. 187 (1999) 151-181.

[43] N. Torapava, L. I. Elding, H. Mändar, K. Roosalu, I. Persson, Dalton Trans. 42 (2013) 7755-7760.

[44] S. F. Lincoln, D. T. Richens, A. G. Sykes, in: Comprehensive Coordination Chemistry II, Pergamon, Oxford, 2003.

[45] R. M. Izatt, D. Eatough, J. J. Christensen, J. Chem. Soc. A: Inorg, Phys, Theor. (1967) 1301-1304.

[46] T. Shi, L. I. Elding, Acta Chem. Scand. 52 (1998) 897-902.

[47] J. Loosdrecht, A. M. Kraan, A. J. Dillen, J. W. Geus, J. Catal. 170 (1997) 217-226.

[48] F. S-S. Chien, Y. T. Wu, G. L. Lai, Y. H. Lai, Appl. Phys. Lett. 98 (2011) 153513.

[49] C-W. Hu, J. Yao, H-Q. Yang, Y. Chen, A-M. Tian, J. Catal. 166 (1997) 1-7.

[50] X. J. Zou, X. G. Wang, L. Li, Int. J. Hydrogen Energy 35 (2010) 12191-12200.

[51] J. Yang; X. G. Wang, L. Li, K. Shen, X. Lu, G. W. Z. Ding, Appl. Catal. B: Environ. 96 (2010) 232-237.

[52] K. Y. Koo, H. S. Roh, Y. T. Seo, D. J. Seo, W. L. Yoon, S. B. Park, Int. J. Hydrogen Energy 33 (2008) 2036-2043.

[53] B. Vos, E. Poels, A. Bliek, J. Catal. 198 (2001) 77-88.

[54] J. M. Rynkowski, T. Paryjczak, M. Lenik, Appl. Catal. A: Gen. 106 (1993) 73-82.

[55] B. Scheffer, P. Molhoek, J. A. Moulijn, Appl. Catal. 46 (1989) 11-30.

[56] J. Sá, G. D. Arteaga, R. A. Daley, J. Bernardi, J. A. Anderson, J. Phys. Chem. B. 110 (2006) 17090-17095.

[57] N. Sheshu Babu, N. Lingaiah, P.S. Sai Prasad, Appl. Catal. Catal. B: Environ. 111-112 (2012) 309-316.

[58] B. Zhou, M. Rueter, US Patent 6,908,873 B2 (2005), to .Headwaters Nanokinetix, Inc.

[59] P. Salagre, J. L. G. Fierro, F. Medina, J. E. Sueiras, J. Mol. Catal. A: Chem. 106 (1996) 125-134.

[60] P. Lu, T. Teranishi, K. Asakura, M. Miyake, N. Toshima, J. Phys. Chem. B. 103 (1999) 9673-9682.

[61] S. A. Krasnikov, A. B. Preobrajenski, T. Chasse, R. Szargan, Thin Solid Films 428 (2003) 201-205.

[62] B. H. Engler, D. Lindner, E. S. Lox, A. Schafer-Sindlinger, K. Ostgathe, Stud. Surf. Sci. Catal. 96 (1995) 441-460.

[63] K. Otto, L. P. Haack, J. E. deVries, Appl. Catal. B: Environ. 1 (1992) 1-12.

[64] K. S. Kim, A. F. Gossman, N. Winograd, Anal. Chem. 46 (1974) 197-200.

[65] D. H. Kim, S. I. Woo, J. M. Lee, O. B. Yang, Catal. Lett. 70 (2000) 35-41.

[66] L. S. Kibis, A. I. Titkov, A. I. Stadnichenko, S. V. Koscheev, A. I. Boronin, Appl. Surf. Sci. 255 (2009) 9248-9254.

[67] P. A. Deshpande, M. S. Hegde, G. Madras, Appl. Catal. B: Environ. 96 (2010) 83-93.

[68] F. Cárdenas-Lizana, S. Gómez-Quero, C. Amorim, M. A. Keane, Appl. Catal. A: Gen. 473 (2014) 41-50.

[69] A.C. Michel, L. Lianos, J.L. Rousset, P. Delichère, N.S. Prakash, J. Massardier, Y. Jugnet, J.C. Bertolini, Surf. Sci. 416 (1998) 288–294.

[70] F.T. Trotta, M. Zanetti, G. Camino, Polym. Degrad. Stab. 69 (2000) 373-379.

[71] L. Bai, F. Wyrwalski, C.Machut, P. Roussel, E.Monflier, A. Ponchel, CrystEngComm. 15 (2013) 2076-2083.

[72] V. N. Belyakov, L. A. Belyakova, A. M. Varvarin, O. V. Khora, S. L. Vasilyuk, K. A. Kazdobin, T. V. Maltseva, A. G. Kotvitskyy, A. F. Danil de Namor, J. Colloid Interface Sci. 285 (2005) 18-26.

[73] A. Lannoy, N. Kania, R. Bleta, S. Fourmentin, C. Machut-Binkowski, E. Monflier, J. Colloid Interface Sci. 461 (2016) 317-325.

[74] E. Grzadka, Colloid. Surf. A: Physicochem. Eng. Asp. 481 (2015) 261-268.

[75] L. Bai, F. Wyrwalski, M. Safariamin, R. Bleta, J-F. Lamonier, C. Przybylski, E. Monflier, A. Ponchel, J. Catal. 341 (2016) 191-204.